LBNL-39506
UC-600
Preprint

ERNEST ORLANDO LAWRENCE BERKELEY NATIONAL LABORATORY

Solute Channeling in Unsaturated Heterogeneous Porous Media

Jens Birkholzer and Chin-Fu Tsang
Earth Sciences Division

September 1996
Submitted to
Water Resources Research

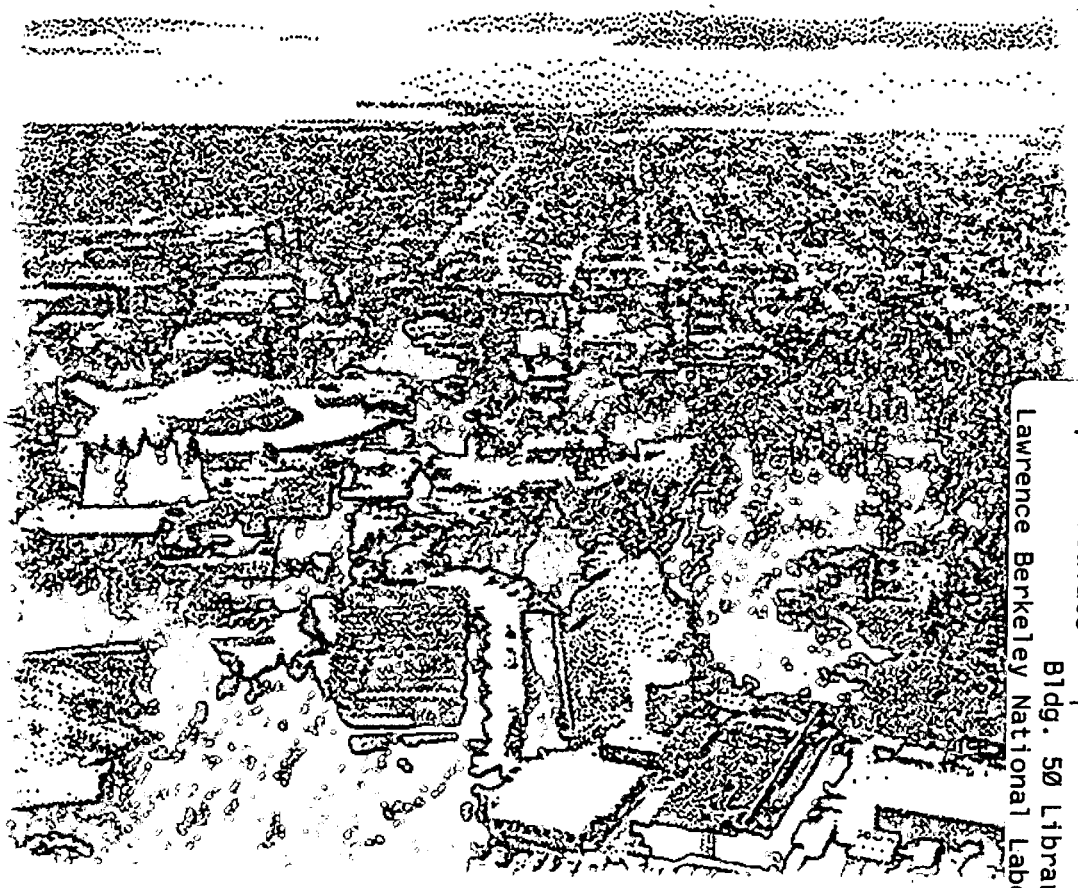

REFERENCE COPY
Does Not
Circulate
Bldg. 50 Library - Ref.
Lawrence Berkeley National Laboratory
Copy 1
LBNL-39506

DISCLAIMER

This document was prepared as an account of work sponsored by the United States Government. While this document is believed to contain correct information, neither the United States Government nor any agency thereof, nor the Regents of the University of California, nor any of their employees, makes any warranty, express or implied, or assumes any legal responsibility for the accuracy, completeness, or usefulness of any information, apparatus, product, or process disclosed, or represents that its use would not infringe privately owned rights. Reference herein to any specific commercial product, process, or service by its trade name, trademark, manufacturer, or otherwise, does not necessarily constitute or imply its endorsement, recommendation, or favoring by the United States Government or any agency thereof, or the Regents of the University of California. The views and opinions of authors expressed herein do not necessarily state or reflect those of the United States Government or any agency thereof or the Regents of the University of California.

LBNL - 39506
UC - 600

Solute Channeling in Unsaturated Heterogeneous Porous Media

Jens Birkholzer and Chin-Fu Tsang

submitted to Water Resources Research

Earth Sciences Division
Ernest Orlando Lawrence Berkeley National Laboratory
University of California
Berkeley, CA 94720

September 1996

This work was supported by a NATO-Postdoctoral Scholarship, provided by the *German Academic Exchange Organization (DAAD),* Bonn, Germany, and a Feodor-Lynen-Postdoctoral Scholarship, provided by the Humboldt-Foundation, given to the first author. It was also partially supported by the Power Reactor and Nuclear Fuel Development Corporation (PNC), Tokyo, Japan, through the U.S. Department of Energy Contract No. DE-AC03-76SF00098.

Solute Channeling in Unsaturated Heterogeneous Porous Media

Jens Birkholzer and Chin-Fu Tsang

Abstract

Numerical simulations have been performed to study flow and solute transport phenomena in strongly heterogeneous porous media. Different saturation scenarios were applied varying from fully saturated to highly unsaturated conditions, corresponding to different infiltration rates into the soil. It was found that the solute travels along preferred flow paths, which may be called channels. This is the case in saturated as well as in unsaturated media. However, the degree of channeling, the location of channels and the hydraulic properties along channels are very much dependent on the mean saturation in the flow domain. Strong channeling effects were obtained in both fully saturated and in low saturation cases. With fully saturated conditions channels develop along zones of high permeabilities; in the case of low saturation we find channels in zones of low permeabilities. Within intermediate saturation ranges, channeling effects are less significant and the system exhibits a more homogeneous flow pattern. The dispersion of solutes as shown in the calculated tracer breakthrough curves essentially reflects the degree of channeling and thus is saturation dependent; in cases when flow channeling is less evident we observe much smaller dispersion than in cases with strong channeling.

1 Introduction

The variation of permeability in a strongly heterogeneous porous medium causes strong variations in the fluid velocities. The fluid seeks to flow in the least resistive paths (channels), and solute traveling along those paths may be transported many times faster than solute traveling in an equivalent homogeneous medium. In practical problems concerning the transport of radioactive or toxic waste, this earlier arrival of contaminants may be of vital importance.

In the last decade channeling phenomena have been intensively studied with regard to ***saturated*** media. *Tsang & Tsang* [1987], *Moreno et al.* [1988, 1990] and *Moreno & Tsang* [1991] investigated the effects of channeling in single fractures with variable apertures. It was found that the hydraulic properties of the channels are different from those of the global porous medium. Also they appeared to be invariant regardless of the actual location of the channels and the overall direction of flow. It was concluded, then, that the characteristics of the entire flow field can be described by the properties of the channels only. *Tsang & Tsang* [1989] and *Moreno & Tsang* [1994] extended their studies to flow and solute transport in two- and three-dimensional porous media with strongly variable hydraulic properties, finding that flow channeling also occurs in such systems. They pointed out that the form of tracer breakthrough curves obtained for pulse injection tests is strongly dependent on the degree of channeling. With increased channeling effects the main peak shifts to much earlier arrival times, indicating that solutes in the channels are transported with much greater velocities than the average velocity of the fluid.

In this paper we focus on flow and solute channeling in ***unsaturated*** porous media. Due to the different hydraulic properties we expect the degree of channeling and the location of channels to be very different from the saturated case, where channels develop along areas of large permeabi-

lity. In unsaturated soil large permeabilities are correlated to large pore volumes, which drain faster than the smaller pores. This can lead to strongly reduced flow rates along zones of high permeabilities, and might completely change the hydraulic structure of the system.

A number of large-scale tracer experiments conducted in the last decade have demonstrated the complexity of flow and transport in unsaturated soil, observing transport phenomena which indicate the existence of flow paths forming a complex network [e.g. *Schulin et al.*, 1987; *Roth et al.*, 1991; *Hills et al.*, 1991; *Hills & Wierenga*, 1991; *Flury et al.*, 1994]. *Roth* [1995] performed numerical simulations of fluid flow in a two-dimensional heterogeneous medium to study possible relations between the saturation of a heterogeneous soil and the phenomenology of the flow. His results show that the structure of the flow network is governed by the degree of saturation in the domain. He was able to identify two states, one with high mean domain saturations, one with low mean domain saturations, which show very different flow characteristics. The two states are separated by a critical saturation at which the flow system becomes almost homogeneous. High-flux regions of one state become low-flux regions of the other state, and vice versa.

In our paper we complement Roth's work by performing a detailed study of flow and solute channeling phenomena in variably saturated media. In particular, we are interested in three questions: (1) Is it possible to find channel properties for given degrees of saturations, which can characterize flow and transport in the entire system ? (2) How do these channels properties compare to the properties of the entire porous medium ? (3) How does the degree of channeling in unsaturated flow affect the transport of contaminants, e.g. with regard to earlier arrival times of solutes and to the dispersion in the system ? To answer these questions numerical simulations of fluid flow and solute transport are performed in a two-dimensional vertical cross-section of a strongly heterogeneous porous medium. Different saturation scenarios are applied varying from fully saturated to highly unsaturated conditions, corresponding to different infiltration rates into the soil.

2 Methodology

Fluid flow and solute transport simulations are carried out for a two-dimensional vertical cross section of a strongly heterogeneous medium (Fig. 1). The model area is 20.0 m wide and 10.0 m deep, representing part of the vadose zone of a porous groundwater system. (However, it may as well represent an area in a vertical single fracture with strongly varying aperture distribution.) Fluid flows with gravity from top to the bottom, the right and left boundaries are closed. Different saturation scenarios are simulated by imposing different capillary pressure values at the upper boundary of the model area. The lower boundary at z=0.0 m coincides with the groundwater table. A steady-state flow field is assumed. The flow field is solved with the multi-component, multi-phase flow simulator TOUGH2 [*Pruess*, 1987 and 1991; *Moridis & Pruess*, 1995], and then a particle tracking procedure is applied to model the transport of contaminants.

The heterogeneity is introduced by dividing the area in 80 x 40 quadratic cells. A permeability value is assigned to each element from a lognormal permeability distribution, with a geometric mean of 10^{-12} m^2 and a standard deviation in $\log_{10}$ of 1.737 (i.e. 4.0 in natural log). Permeability correlation in space is isotropic with a correlation length of 0.5 m and is imposed using an exponential autocovariance model. Then, the characteristic length of regions with similar hydraulic properties is in the range of 1.5 m (effective correlation range). The random permeability fields are calculated with the numerical code COVAR which uses the covariance matrix decomposition method [*Williams and El-Kadi*, 1986]. Three different realizations of random fields are generated. The porosity in the model area is constant, with a value of 0.35.

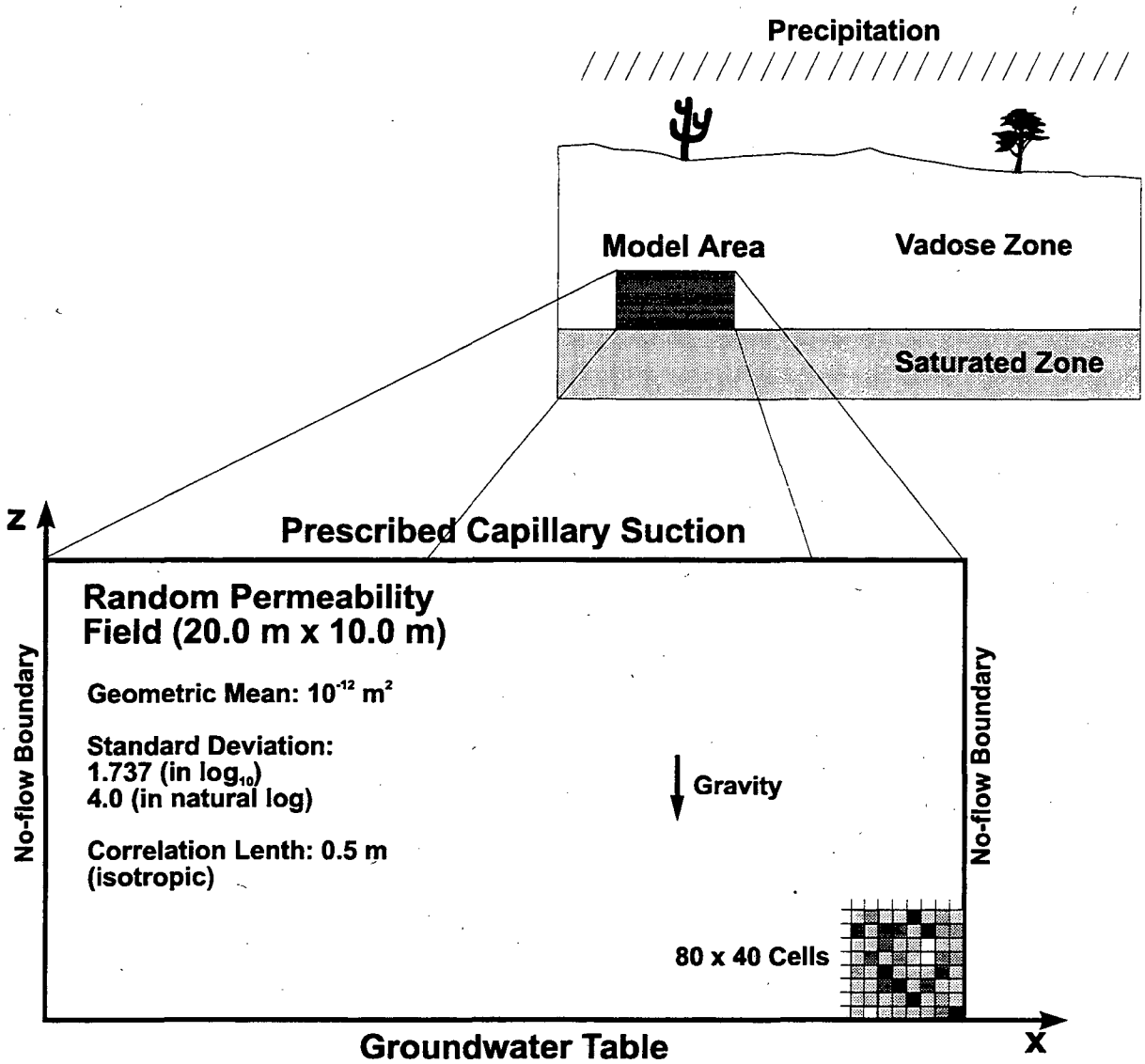

Fig. 1: Model area

2.1 Flow Simulation

The flow simulations are performed with the numerical simulator TOUGH2, developed at the Berkeley Laboratory [*Pruess*, 1987 and 1991, *Moridis & Pruess*, 1995]. TOUGH2 is a widely used code for nonisothermal flow of multicomponent, multiphase fluids in porous and fractured media. The governing equations are integrated in space using an integral finite difference formulation. In our study only a small part of TOUGH2's capabilities are used, since only one phase (liquid) and one component (water) under isothermal conditions is taken into account. It is assumed that the air phase is immobile, so only the movement of water has to be calculated. The pressure in the air phase is constant (reference pressure P_r). Under the assumption of constant porosity, liquid density and liquid viscosity, the flow of water in the unsaturated zone can be described by a liquid mass balance equation as follows

$$\phi\, \rho \frac{\partial S}{\partial t} - \nabla \left\{ k \frac{k_r}{\mu} \rho \nabla \left[P + \rho g z \right] \right\} = 0 \ . \qquad (1)$$

Here ϕ is porosity, S is saturation, ρ is density, k is permeability, k_r is relative permeability, μ is viscosity, $P = P_r + P_{cap}$ is pressure (sum of reference pressure P_r and capillary pressure P_{cap}), and g is gravitational acceleration. The z-coordinate axis points vertically upwards. Note that Eq. (1) represents a form of Richards' equation; however, the notation used is slightly different since it is based on multi-phase flow concepts [*Oldenburg & Pruess*, 1993].

Both capillary pressures and relative permeabilities depend on the saturation, and characteristic functions are used to describe these relations. In our study, we use the well-known van Genuchten-Mualem capillary pressure and relative permeability model, given as [*van Genuchten*, 1980; *Mualem,* 1978]

$$P_{cap}(S_e) = -P^*\left\{(S_e)^{-n/(n-1)} - 1\right\}^{1/n} \tag{2}$$

$$k_r(S_e) = (S_e)^{0.5}\left\{1-\left(1-(S_e)^{n/(n-1)}\right)^{1-1/n}\right\}^2 \tag{3}$$

with the effective saturation defined as

$$S_e = (S - S_r)/(1 - S_r). \tag{4}$$

Here S_r is the residual saturation, P^* is a scaling factor for the capillary pressure function and n characterizes the distribution of pore sizes within each grid element ($1 < n < \infty$).

In a heterogeneous porous medium, the characteristic functions of capillary pressure and relative permeability may not be spatially constant. As already mentioned, areas of high permeability are expected to drain faster, due to large pore sizes and less capillary strength. Likewise, areas of low permeability are expected to maintain larger water saturations, due to smaller pore sizes and stronger capillary suction. Consequently, areas with different permeabilities in our model region have to be assigned different capillary pressure functions. This is done by using spatially varying scaling factors P^* for the capillary pressure function in Eq. (2). *Leverett* [1941] proposed a model to calculate the scaling factor P^* at a given location with permeability k as follows

$$P^* = \overline{P}^*\left(\overline{k}/k\right)^{0.5} \tag{5}$$

where $\overline{k}$ and $\overline{P}^*$ are reference values for the permeability and the scaling factor, respectively. A number of workers have shown that relationship in Eq. (5) holds for a variety of different soils [e.g. *Davies,* 1991; *Wang,* 1992].

A special TOUGH2 version was developed to simulate the heterogeneity in capillary suction [*Finsterle et al.,* 1994]. For each cell of the model region the scaling factor P^* is calculated from Eq. (5) according to the particular permeability value in the cell. After introducing the different values of P^* into Eq. (2) a different capillary pressure function is assigned to each cell, and Eq. (1) can finally be solved considering the spatial variation in capillary suction.

In our study the reference values for the scaling law in Eq. (5) are given as 10^{-12} m^2 for permeability $\overline{k}$ (equal to the geometric mean) and 10,000 Pa for the scaling factor $\overline{P}^*$. For the sake of simplicity we assume that the spatial variability of pore sizes does not change from cell to cell within the model area. Then, the pore size distribution coefficient n is not modified, and this allows the relative permeability function in Eq. (3) to be constant over the whole model area. We choose a pore size distribution coefficient of 2.0 and a residual saturation of 0.2. All values represent parameter ranges which are typical for data observed in field experiments.

Figure 2 shows three different capillary pressure functions for permeability values of 10^{-9} m^2, 10^{-12} m^2 and 10^{-15} m^2, respectively, calculated using Eqs. (2) and (5). It is immediately evident

that regions with different permeabilities show significant differences in their hydraulic behavior. For example, in a cell with the mean permeability of 10^{-12} m^2 a capillary pressure of -25,000 Pa is associated with a water saturation of 0.5. However, in a low permeability cell ($k = 10^{-15}$ m^2), the same capillary force is associated with almost full water saturation. For high permeabilities ($k = 10^{-9}$ m^2), the saturation drops to almost the residual saturation, the cell is drained.

Figure 3 shows the relative permeability function, calculated using Eq. (3). It represents the typical hydraulic behavior of unsaturated soils, with the relative permeabilities rapidly decreasing when saturation is close to the residual saturation. As already mentioned, the relative permeability function is the same for the whole model area.

The relation between relative permeability and capillary pressure is depicted in Figure 4, again presented for permeabilities of 10^{-9} m^2, 10^{-12} m^2 and 10^{-15} m^2, respectively. Comparison of the three curves shows that for a given capillary suction the relative permeability in high permeability zones is much smaller than in low permeability zones. As shown in Figure 5, this has a strong effect on the product of permeability k and relative permeability k_r which gives the effective value of permeability for unsaturated flow. To clearly distinguish between the different terms, we like to introduce the term "absolute permeability" for the permeability k of the soil. The product of absolute permeability k and relative permeability k_r is referred to as "effective permeability". For small values of capillary suction, which correspond to almost saturated soil, the effective permeability in high absolute permeability zones is higher than the effective permeability in low absolute permeability zones. However, this changes when the capillary suction increases as the soil is desaturating. Because of their larger pores, high absolute permeability zones drain earlier, and the effective permeability drops to negligible values. As a consequence, the hydraulic structure of a heterogeneous soil may be totally reversed. High flux zones in nearly saturated soil become low flux zones in highly unsaturated conditions, and vice versa.

2.2 Solute Transport Simulation

After solving the flow field and calculating particle velocities in each cell, a particle tracking procedure is performed to model the transport of contaminants through the porous medium. A total number of 300 particles is released at the inflow cells of the upper boundary. Some simulation runs have been performed with two or three times the number of particles to check the sensitivity of the model results. It has been shown, however, that a total number of 300 particles is sufficient to provide stable results. The number of particles to be introduced in each inflow cell is proportional to the specific discharge into that cell. Within each inflow cell, particles are randomly distributed along the upper boundary. Each particle is then followed from these inflow cells through the model area until it reaches the bottom.

We use a particle tracking technique implemented in the interactive plotting software TECPLOT [*TECPLOT*, 1995] which features a predictor-corrector integration scheme to trace particles through a vector field. First, the velocity at the current particle location is linearly interpolated from the adjacent data points. A step is taken in the direction of the velocity vector to a tentative new point. A minimum step size of 2.5 % of the actual cell size and a maximum step size of 25 % of the actual cell size is used in our study. TECPLOT chooses an appropriate step size within these limits according to the velocity gradient. Then, new velocity components are interpolated at the new tentative point. Now using the average of the velocities at the new and the original point, the step is redone from the original point and this corrects the first estimate. No local dispersion is considered in this scheme.

During the particle tracking process, a number of parameters are recorded along the trace, such as absolute and relative permeabilities or saturations. These data are used to calculate statistics of the flow path properties and compare them to the statistics of the entire porous medium. Eventually particles are collected at the bottom boundary, and the travel time for each particle is calculated to derive tracer breakthrough curves. Following *Moreno & Tsang* [1994], all these calculations are based on the fastest 90 % of particles. This is reasonable (1) because from the contamination point of view the early arrival and the main part of solute are more significant, (2) because contaminants may decay within long travel times, and (3) because the slowest part of solute is often several orders of magnitude slower than the main part and will often not be measured in any practical field situations.

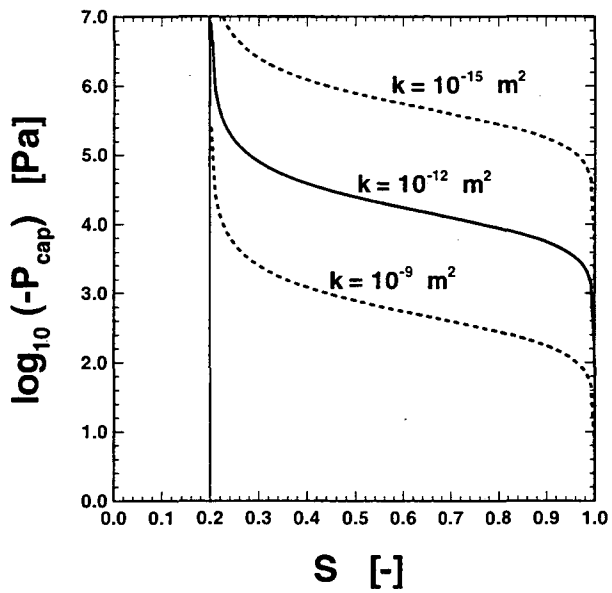

Fig. 2: Capillary pressure as a function of saturation

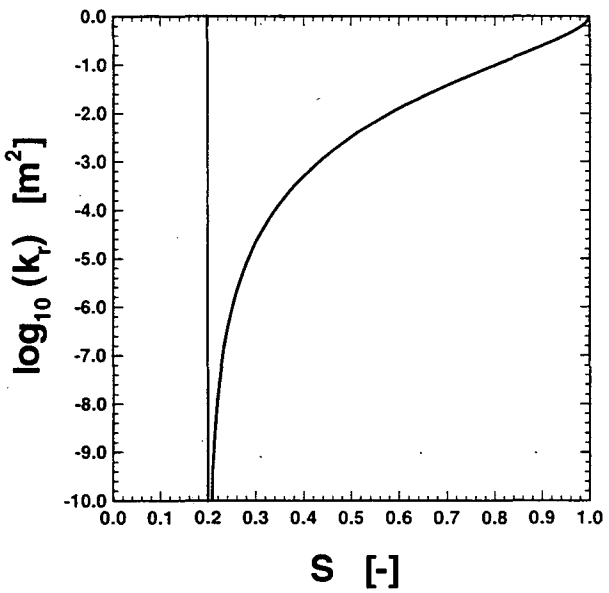

Fig. 3: Relative permeability as a function of saturation

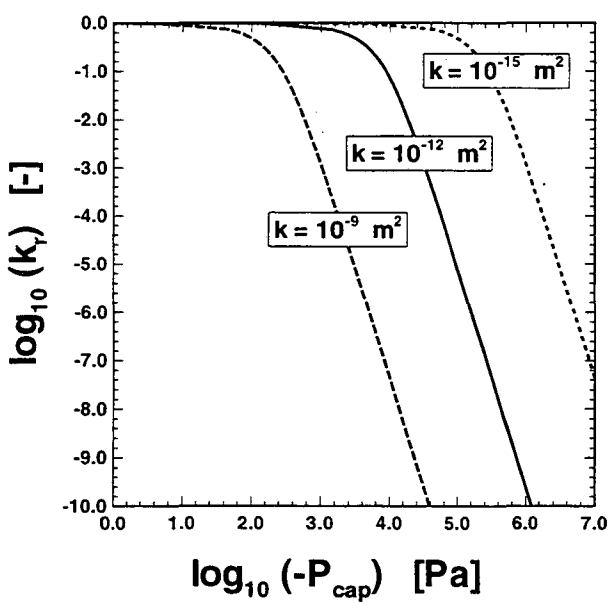

Fig. 4: Relative permeability as a function of capillary pressure

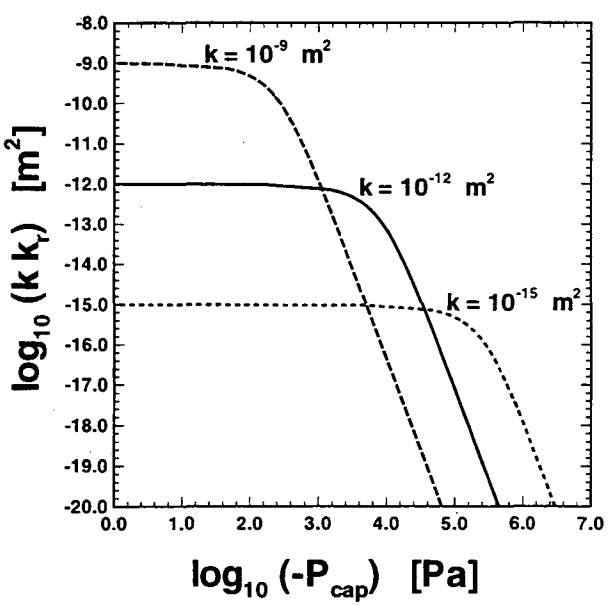

Fig. 5: Effective permeability as a function of capillary pressure

3 Simulation Runs and Results

Five saturation scenarios are used to study solute channeling in heterogeneous media. Four of them represent different unsaturated flow conditions (*Cases U1, U2, U3* and *U4*), one represents fully saturated flow conditions (*Case S*). The fully saturated case is mainly included for the sake of comparison. In this case, we apply a zero pressure difference between the top and the bottom boundary; i.e. gravity is the driving force for water flow.

The unsaturated scenarios are simulated with uniform capillary pressures applied along the top boundary of the model area. Different values of capillary pressures at the boundary correspond to different infiltration rates into the model area: large capillary suctions are associated with low saturation values and low infiltration rates, small capillary suctions are associated with high saturation values and high infiltration rates. Note that a uniform capillary pressure along the top boundary gives rise to a non-uniform distribution of infiltration rates, i.e. the flow into the model area is distributed according to the actual effective permeability and gradient at each boundary cell. Thus, with the uniform capillary suction boundary, flow channels originate right at the surface while with a uniform flux boundary they could only form at some distance from the surface. The latter does not coincide with the conceptual model of the flow region which represents a part of a large natural flow system, with the inflowing water following preferred flow paths.

The numerical treatment of the upper boundary condition needs some attention. Assigning capillary pressure values at the upper boundary would mean that the average infiltration into the model area comes out as a simulation result. As a consequence, the infiltration rates cannot be assigned prior to a simulation run, and the values calculated for different realizations of the random field might vary significantly although the same capillary suction boundary condition is applied. However, we want to discuss our simulation results with regard to the infiltration rate, i.e. prescribed infiltration rates should be imposed for the different realizations. To realize that in the numerical simulation, we add a new layer of elements at the periphery of the top boundary cells with an absolute permeability equal to the geometric mean of the flow domain. We artificially assign a large horizontal flow capacity to these additional cells and impose a uniform infiltration rate at the new element layer. Then, the large horizontal flow capacity of this layer allows the infiltrated water to be distributed to the cells of the top boundary according to the actual effective permeability and gradient in each cell. Having specified the infiltration rate, this procedure guarantees that the upper boundary is associated with a uniform capillary suction and a non-uniform ("channeled") distribution of fluxes.

The bottom boundary condition at $z = 0.0$ m corresponds to the groundwater table, i.e. $S = 1.0$ and $P_{cap} = 0.0$ Pa. We are mainly interested in shallow groundwater systems, and in the variably saturated zone close to the groundwater level. According to findings of *Faybishenko* [1995] the phenomenon of entrapped air can significantly influence the hydraulic behavior in areas where water saturations are very large. Thus, the assumption of a passive air phase may not be justified close to the lower boundary of our model region, in particular when simulating transient flow processes and studying the transition between different saturation scenarios. However, as we limit our study to steady-state flow conditions we do not address the problem of entrapped air.

Table 1 lists the infiltration rates Q_{inf} chosen for the four unsaturated cases. They are given as relative values, i.e. the actual infiltration rate Q_{inf} is divided by a flow rate Q_{inf}^{sat} which denotes the theoretical water flow between the top and bottom boundary under fully saturated conditions, assuming that the model area is homogeneous with $\bar{k} = 10^{-12}$ m^2. *Case U1*, with the lowest infiltration rate, represents a highly unsaturated flow field. Then, with increasing infiltration rates, *Cases U2, U3* and *U4* represent scenarios with intermediate to high mean domain saturations.

	Case U1	Case U2	Case U3	Case U4
Q_{inf} / Q_{inf}^{sat}	10^{-5}	10^{-3}	10^{-2}	10^{-1}

Table 1: Infiltration rate for different scenarios (with $Q_{inf}^{sat} = \bar{k}\ \rho^2 g / \mu$)

Starting with initially uniform saturations, TOUGH2 flow simulations are performed until a steady-state flow condition is reached. To check the sensitivity of our results we used three grid sizes of the finite difference mesh: 80 x 40 cells, 160 x 80 cells and 240 x 120 cells, with the correlation length covered by two, four and six cell lengths, respectively. Our simulations indicate that the results are not very sensitive to the discretization. Local saturation and capillary pressure values show minor differences, while the location and statistics of channels are not affected at all.

An important point in finite difference modeling of heterogeneous fields is the choice of weighting schemes for flow between two adjacent blocks of different permeabilities. For single-phase flow, the appropriate weighting scheme for absolute permeability is harmonic weighting. For two-phase flow (or unsaturated flow), a second weighting scheme has to be chosen for the relative permeabilities. *Pruess* [1991] recommends upstream weighting of both absolute and relative permeabilities in case of transient flow; for steady-state flow, however, a harmonic weighting of the effective permeabilities is favored. In order to check the sensitivity of the model results, we performed TOUGH2 runs with both weighting schemes. It was found that the differences between the two weighting schemes were minor and much smaller than the differences between realizations. All results presented in this paper are calculated with a fully harmonic weighting scheme.

3.1 Flow Field

As we mentioned above, calculations were carried out for three different realizations of the random absolute permeability field. One particular realization is chosen here to present spatial distributions of saturation, capillary pressure, hydraulic head, flow rate, and effective permeability for the different test cases, with *U1, U2, U3* and *U4* labeling the four unsaturated cases and *Case S* being the fully saturated case. The spatial distribution of absolute permeabilities for the particular selected realization is depicted in Figure 6.

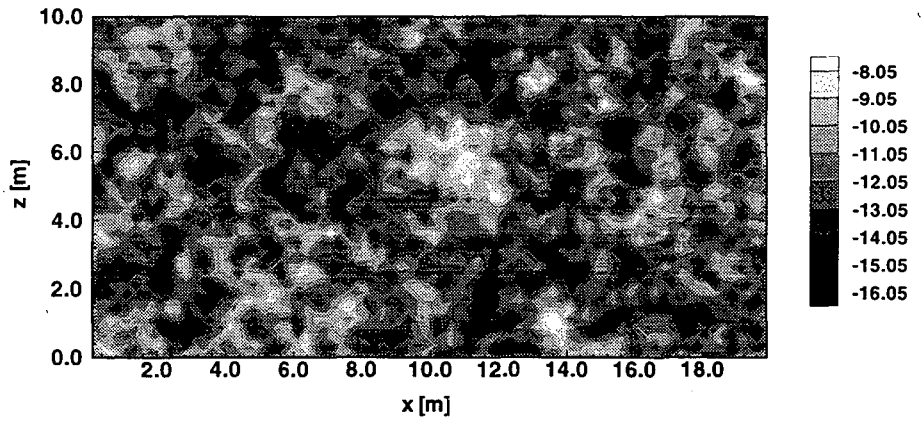

Fig. 6: Spatial distribution of absolute permeability (in $\log_{10} m^2$)

Note that the actual geometric mean and standard deviation of the generated absolute permeability field in Figure 6 does not exactly match the input for the random field generator COVAR [*Williams & El-Kadi*, 1986]: The actual values of the random field are $\log_{10} \bar{k} = -12.05\ m^2$ and $s = 1.616$ versus input values of $\log_{10} \bar{k} = -12.00\ m^2$ and $s = 1.737$. The contour values are chosen to cover eight orders of magnitude, with the mean contour level equal to the geometric mean of absolute permeability.

Spatial Distribution of Hydraulic Variables

We will first discuss the results of the fully saturated *Case S*, which form the basis for comparison with the results of the four unsaturated scenarios. Figure 7 shows the magnitude of water flux in the model area. This allows for a visual interpretation with regard to the degree of channeling and the location of channels. All values are relative flow rates, defined as the magnitude of water flux divided by the infiltration rate Q_{inf}^{sat}. The contour intervals are defined by dividing the full range of values into equal steps.

As expected from previous studies regarding channeling phenomena in saturated media [e.g. *Tsang & Tsang*, 1989; *Moreno & Tsang*, 1994], the majority of flow takes place in a few selected pathways while a major part of the model area exhibits very low flow rates. It seems reasonable to refer to these preferred flow paths as tortuous one-dimensional channels, and to describe the flow field in the model area based on the properties of those channels rather than on the properties of the entire porous medium. A comparison of Figure 6 and Figure 7 indicates that the channels develop along interconnected zones of high absolute permeabilities; the fluid seeks to flow in the least resistive pathways.

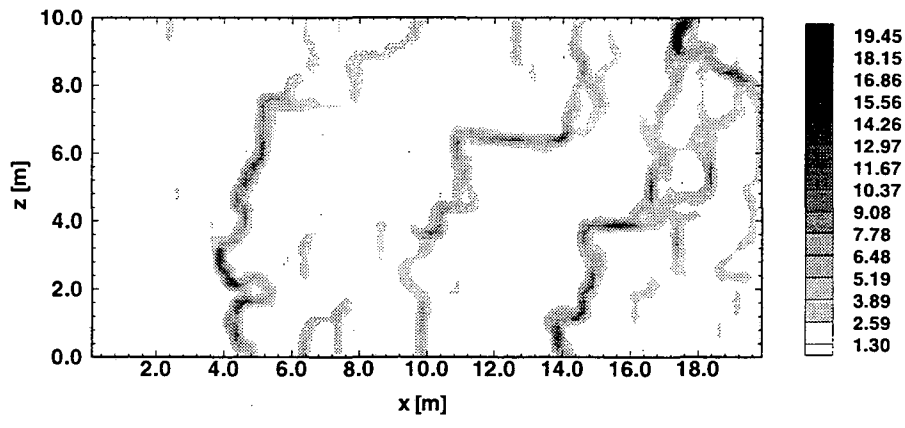

Fig. 7: Spatial distribution of relative flow rate for the saturated *Case S*

In the following section, we present simulation results for the unsaturated flow scenarios. Let us first discuss the hydraulic properties of the four test cases in a more general manner to identify the differences resulting from the different infiltration rates Q_{inf}. Figures 8, 9 and 10 show the vertical distribution of saturation, capillary pressure and hydraulic head, respectively. All values are averaged over the width of the model area. (The reference pressure P_r is chosen to 0.0 Pa.) *Case U1*, with the lowest infiltration rate, is associated with a low saturation, strong capillary suction and a relatively small gradient of hydraulic head. In contrast, high infiltration rates as in *Case U4* lead to a high saturation and small capillary suction. Here, the gradient of hydraulic head is larger; it essentially reflects the effect of gravity. The arithmetic mean of saturation is 0.52 for *Case U1*, 0.60 for *Case U2*, 0.70 for *Case U3* and 0.84 for *Case U4*.

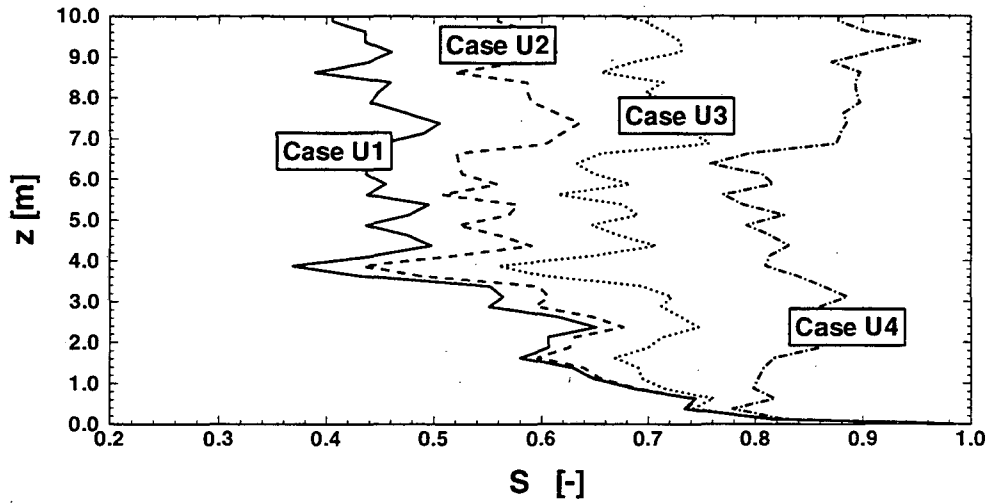

Fig. 8: Vertical saturation profile, values averaged over width of model area

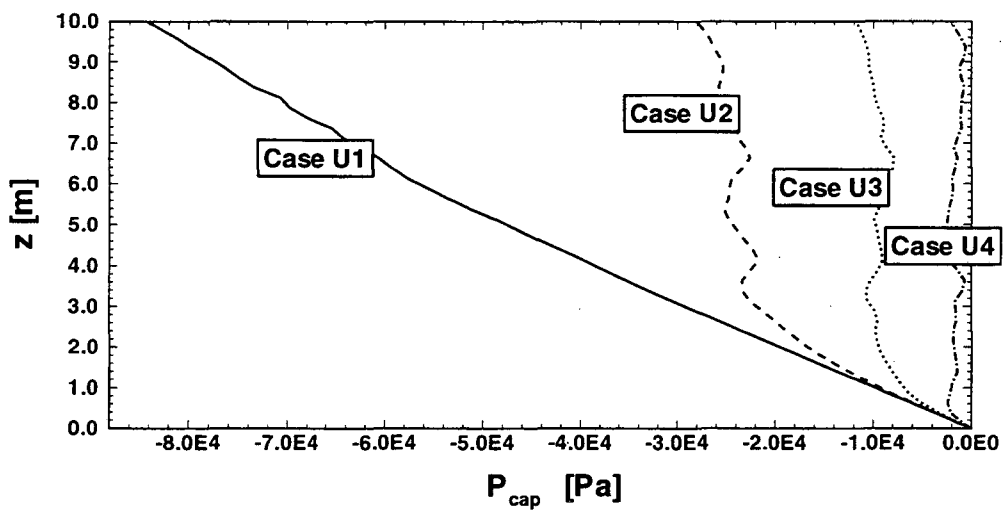

Fig. 9: Vertical capillary pressure profile, values averaged over width of model area

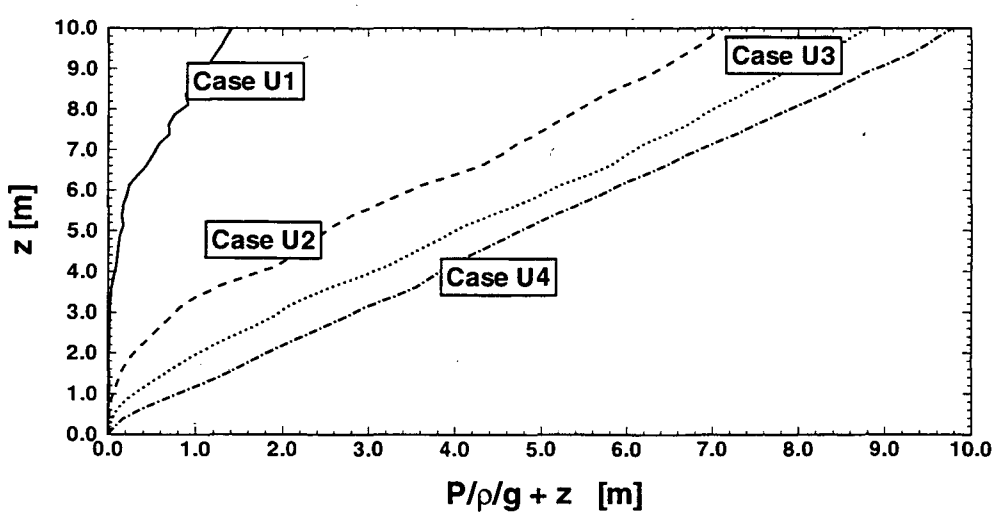

Fig. 10: Vertical profile of hydraulic head, values averaged over width of model area

All curves in Figures 8, 9 and 10 are obviously affected by the groundwater table at z = 0.0 m, with prescribed variables of S = 1.0 and P_{cap} = 0.0 Pa along the bottom boundary. For *Cases U2, U3* and *U4* this effect vanishes at a certain distance from the groundwater table; the saturation and capillary pressure values are macroscopically uniform outside of this boundary region, and the gradient of hydraulic head is almost constant. Thus, the upper region of the model area may represent the vadose zone of a hydrogeological system which is not influenced by the groundwater table. In *Case U1*, however, both saturation and capillary pressure vary over the whole depth of the model area, and the gradient of hydraulic head increases with the distance from the groundwater table. Here, the whole flow domain is sensitive to the lower boundary and hence is completely located in a transition zone between the groundwater table and the vadose zone. At the end of this paper, we will briefly demonstrate that the main findings of our numerical study also hold for deep groundwater systems where the area of interest is not influenced by the groundwater table.

The saturation profiles of all test cases in Figure 8 show very strong local variations while the capillary pressure profiles in Figure 9 and the hydraulic head profiles in Figure 10 are much smoother. This is a typical observation in unsaturated flow systems, originated in the physics of unsaturated flow [*Roth*, 1995]. The gradient of hydraulic head, essentially determined by capillary pressure and gravity effects, is the driving force for water flux, and this flux has the tendency to minimize the gradient. The saturation S has no function as a driving force; it is basically determined by the capillary pressure at a certain location, with the relation between S and P_{cap} given by the capillary pressure function in Eq. (2). Since P_{cap} varies only slowly in space, the spatial variation of S reflects the spatial variation of the capillary pressure function, given by the scaling law in Eq. (5). Note that all saturation profiles shown in Figure 8 have a similar pattern of local variation, due to the fact that the same heterogeneous field is used.

Figure 11 shows the spatial structure of the saturation fields for *Cases U1, U2, U3* and *U4*. As already observed in Figure 8, the impact of the different infiltration rates Q_{inf} is immediately evident: *Case U1* is associated with a low mean domain saturation, showing large areas close to the residual saturation. In contrast, *Case U4* has a high mean domain saturation, with major parts of the model area fully saturated. In all cases the spatial structure of the calculated saturations reflects the heterogeneity of the absolute permeability field in Figure 6. Zones of low absolute permeability correlate with high saturation values while high absolute permeability zones exhibit low saturations. The observed saturation values cover almost the entire possible range between the residual saturation S_r = 0.2 and the maximum saturation S = 1.0. Even in *Case U4*, with a high mean domain saturation, the minimum value is S = 0.21, indicating a strong heterogeneity of the saturation field.

As the relative permeabilities in unsaturated media are strongly dependent on saturation, we may expect major changes in the hydraulic structure of the system. Figure 12 shows the spatial distribution of effective permeabilities in the model area. The contour intervals are identical in all cases to allow for a comparison between the different permeability fields. We choose the same contour intervals as used in Figure 6 for the absolute permeabilities; the contour values cover eight orders of magnitude, with the mean contour level equal to the geometric mean of the effective permeability.

Let us first discuss *Case U1*, the low saturation case. The effective permeability field appears to be as heterogeneous as the absolute permeability field shown in Figure 6. However, the hydraulic structure is completely reversed. Due to their low saturation, zones of high absolute permeability now have the lowest effective permeability, and vice versa. Apparently, the relative permeability values according to Eq. (3) drop so rapidly with decreasing saturation that even-

tually the effective permeabilities of low saturation zones become almost negligible, despite of their high absolute permeability values.

In *Case U2* we observe a similar spatial distribution of the effective permeabilities as in *Case U1*; the two cases seem spatially correlated. For example, both cases show a very typical pattern of low effective permeability zones in the center of the model area. However, the hydraulic field in *Case U2* seems less heterogeneous than in *Case U1*. Apparently, the degree of heterogeneity decreases with increasing saturation. This trend is even more evident in *Case U3*. Here, most of the effective permeabilities seem to be in a small range around the geometric mean, as it is typical for homogeneous media. Cases with an intermediate degree of saturation seem to display a natural smoothing effect with regard to the fluctuations in effective permeability values.

The results for *Case U4*, however, show that a further increase in infiltration rates and mean domain saturation does not lead to a further homogenization. On the contrary, the variation of effective permeabilities in *Case U4* seems slightly larger than in *Case U3*. Another interesting point is the spatial structure of the effective permeability field: some parts of the model area show a correlation with the other unsaturated cases (i.e. areas with low saturation); in other parts, however, the hydraulic structure is more similar to that of *Case S* (i.e. areas with high saturations, e.g. close to the left boundary of the model area). Obviously, *Case U4* represents a transition scenario between predominantly unsaturated conditions as in *Cases U1, U2, U3* and fully saturated conditions as in *Case S*.

Figure 13 shows the flow fields calculated for the different unsaturated cases. As in Figure 7 for *Case S*, we present relative values for the magnitude of flux, with the actual value divided by the infiltration rate Q_{inf} of the particular test case. In all cases we define the contour values by dividing the range of actually occurring flow rates into equal intervals.

The distribution of flow rates reflects the heterogeneity of the effective permeability fields, as presented in Figure 12. For *Case U1*, with low mean domain saturation and strongly varying effective permeabilities, channeling effects are very obvious: Only a few selected pathways develop in the model area. Here, the degree of channeling seems similar to that of the fully saturated *Case S* (compare to Fig. 7). However, the location of channels is very different. In *Case S* preferred flow paths correlate to high absolute permeabilities, while in *Case U1* channels develop along interconnected zones of higher saturation which now correspond to zones of low absolute permeabilities.

In *Cases U2, U3* and *U4*, with a higher degree of saturation and less variation in effective permeability, the ratio between maximum and minimum flux is much smaller than in *Case U1*. Especially in *Cases U3* and *U4* we observe an almost homogeneous flow pattern. Also, the direction of flow is predominantly vertical, indicating that the conducting zones are well connected. This is different in cases with pronounced channeling effects as in *Cases U1* and *S*. In the latter two cases, the flow paths are very tortuous and include parts with predominantly horizontal flow, apparently because low-permeability zones block the direct vertical connection.

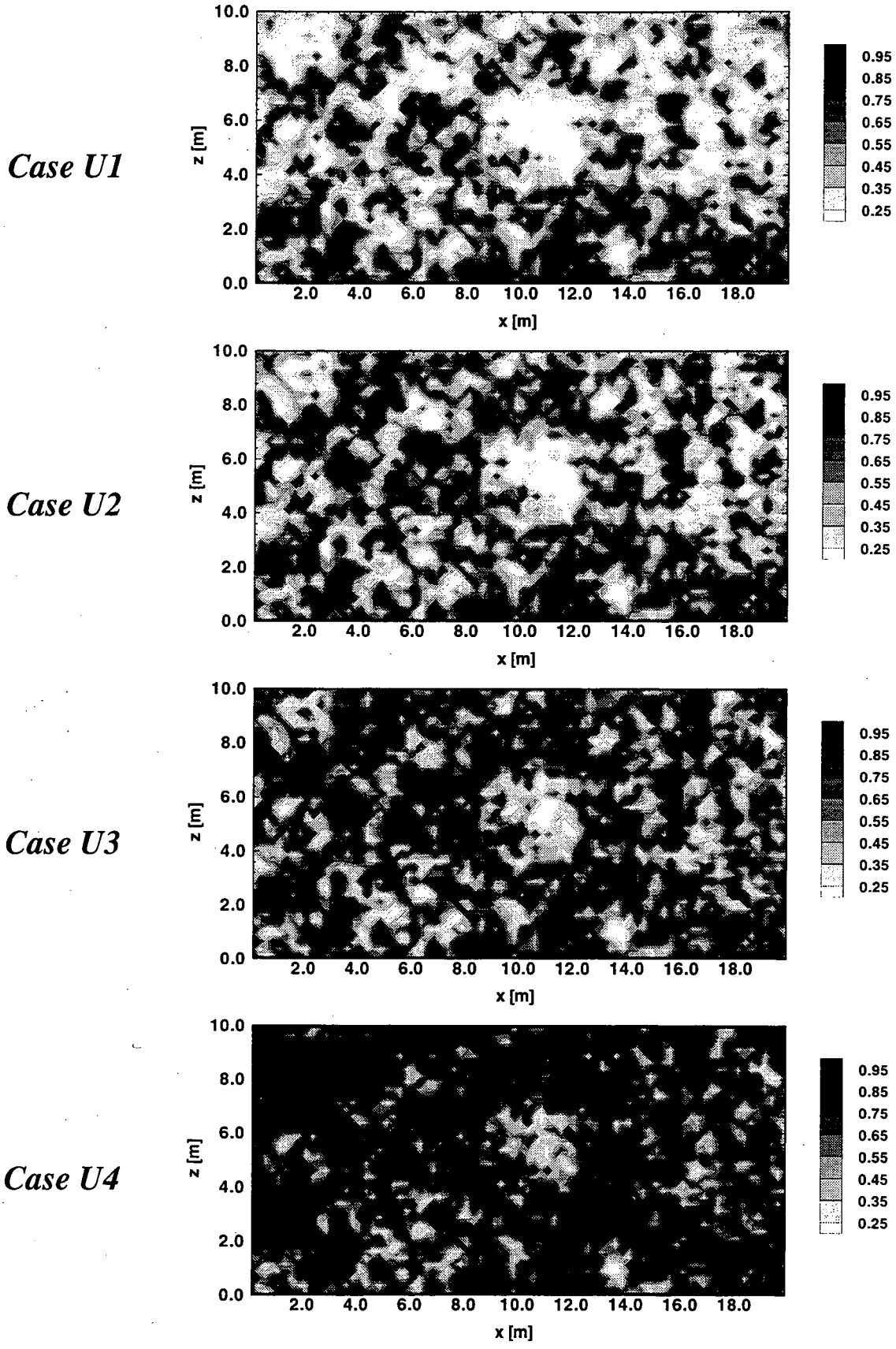

Fig. 11: Spatial distribution of saturation for different test cases

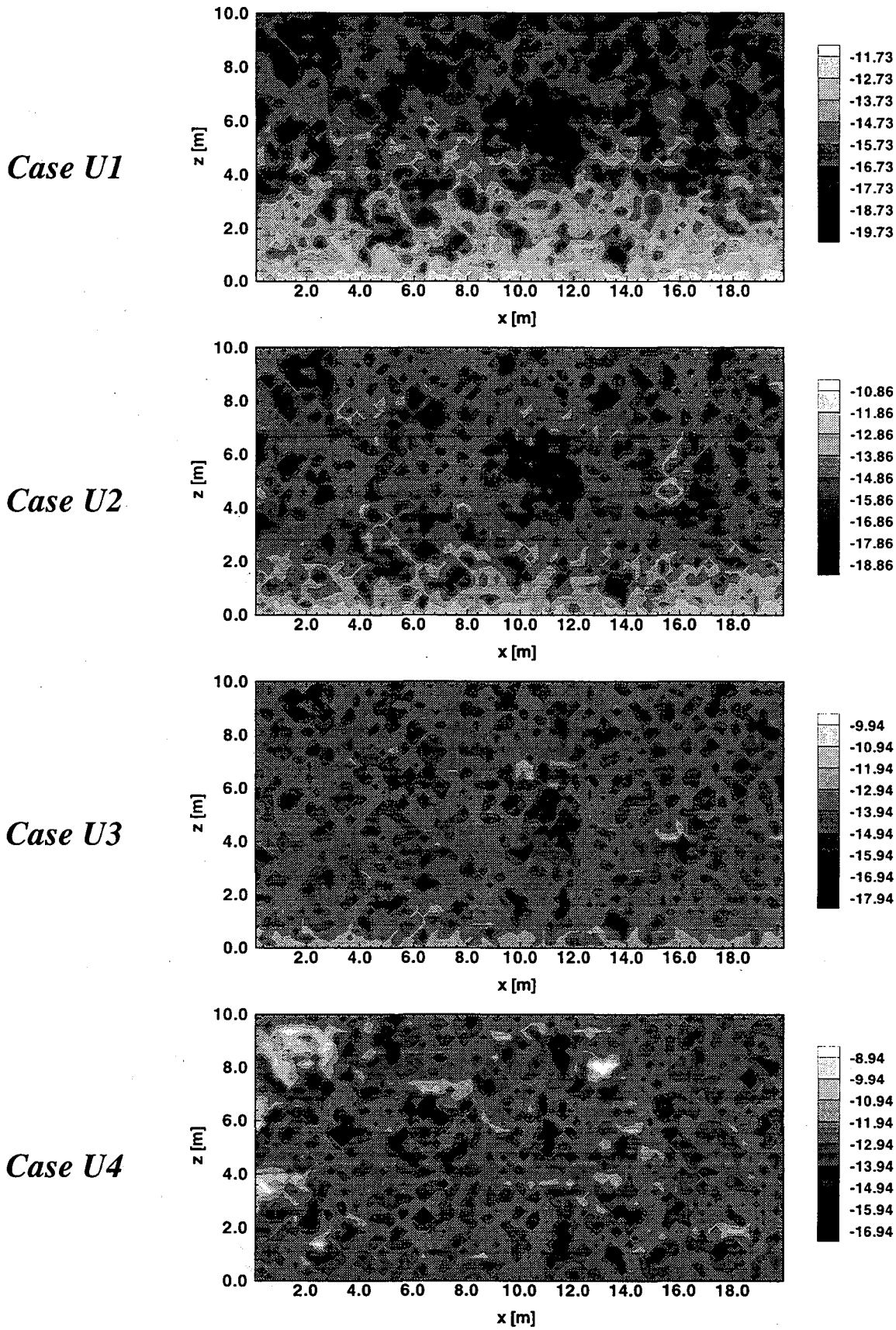

Fig. 12: Spatial distribution of effective permeability for different test cases (in $\log_{10} m^2$)

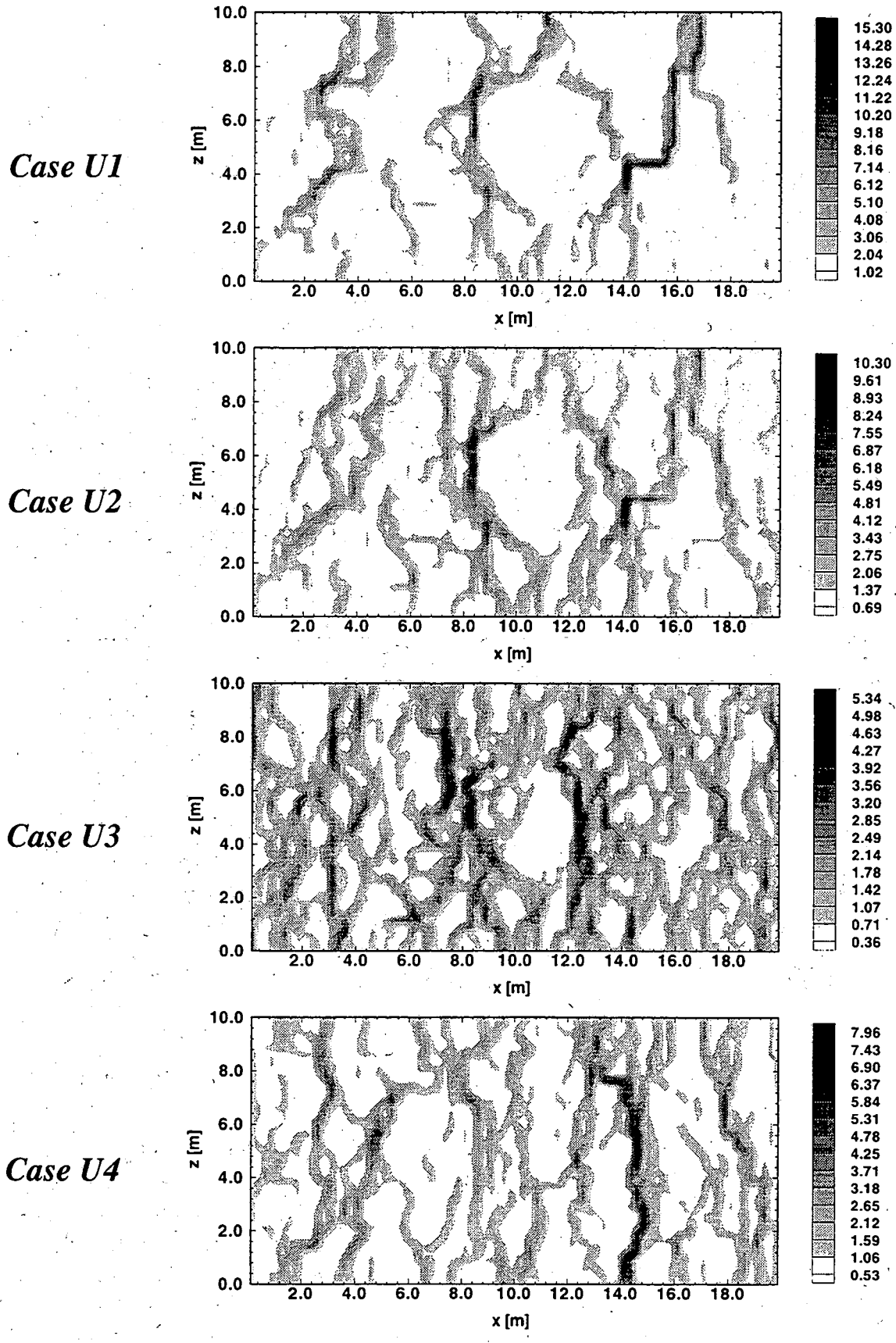

Fig. 13: Spatial distribution of relative flow rate for different test cases

Statistics of Hydraulic Variables

In the next section we will analyze the statistics of effective permeabilities to support the more visual interpretation presented in the last paragraphs. Figure 14 shows the frequency distributions for the different test cases, Figure 15 presents the respective standard deviations. To get a more complete picture we include results of all three realizations. In both figures, the differences between realizations appear to be much smaller than the differences between particular test cases.

Naturally, the frequency distributions in Figure 14 are strongly dependent on the infiltration rates and the mean domain saturation. The lowest effective permeabilities are obtained in *Case U1*, associated with a very low infiltration and a low degree of saturation. Then, with increasing infiltration, the frequency distributions shift to higher effective permeabilities, with the maximum values found for the fully saturated *Case S*. Note that in the latter case the effective permeability distribution is equal to the absolute permeability distribution.

An interesting point is the shape of the frequency curves. In *Case U1* and *Case S* we find very broad distributions, indicating the strong heterogeneity of the hydraulic fields. In the other cases, the frequency distributions are more narrowly peaked, corresponding to a less heterogeneous medium. Almost all distributions appear asymmetric, with the peak frequency in the upper range of values and a tail of small frequencies in the lower range of values. Only the effective permeability distributions of *Case S* are symmetric since they essentially represent the lognormal distribution provided by the random field generator.

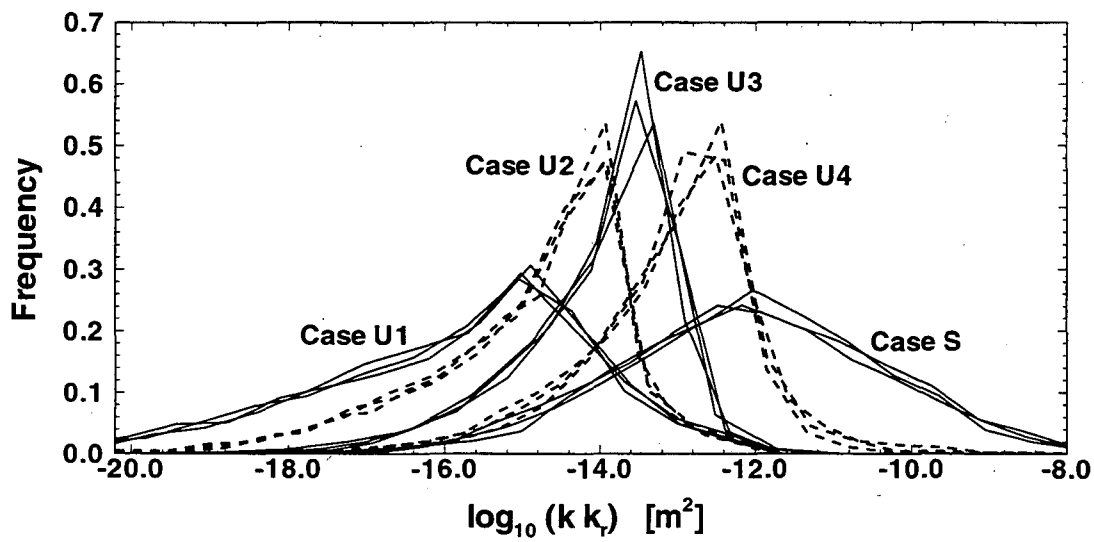

Fig. 14: Frequency distribution of effective permeability, for three realizations of the heterogeneous field

The standard deviations presented in Figure 15 summarize the results of the statistical analysis. The standard deviations of the low saturation *Case U1* and the fully saturated *Case S* are in the same high range, both representing very heterogeneous fields. Resulting from these heterogeneities are the strong channeling effects for both scenarios, as shown in Figures 7 and 13, respectively. In cases with intermediate saturations, however, the standard deviations drop significantly; the flow system becomes more homogeneous. In particular, *Cases U3* and *U4* represent an intermediate range of heterogeneity where, according to previous studies, channeling effects are less evident [*Moreno & Tsang*, 1994]. These findings are essentially consistent with the results of *Roth* [1995]; minor differences are mainly due to differences in the parameters chosen for the

simulation runs. In our study the heterogeneity and spatial correlation of the random field is much higher; further differences occur in the characteristic functions, boundary conditions and numerical solution techniques used.

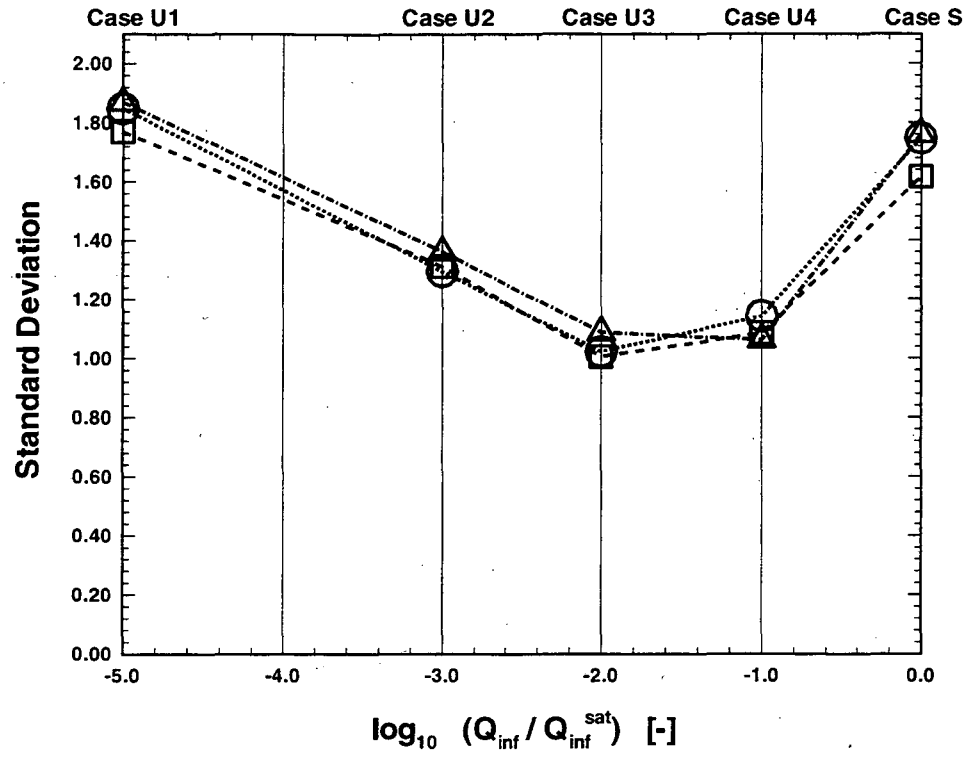

Fig. 15: Standard deviation of effective permeability (in $\log_{10} m^2$) as a function of the infiltration rate, for three realizations of the heterogeneous field

An interesting question is whether, in addition to the mean and standard variation, the spatial correlation of effective permeabilities also changes with the infiltration rate. Figure 16 presents semi-variograms for the different cases and the three realizations of the random field. The dotted curves show the semi-variograms calculated in x-direction, and the dashed curves show the semi-variograms calculated in z-direction. *Cases U3*, *U4* and *S* have an isotropic spatial correlation while in *Case U1* and, less obviously, in *Case U2* the variances in z-direction are higher than in x-direction. This is due to the lower "groundwater table" boundary condition; in *Cases U1* and *U2* its impact is stronger than in the other cases (compare to Fig. 8, 9 and 10).

The semi-variogram for *Case S* represents the spatial correlation of the absolute permeability fields, as provided by the random field generator. It reaches its sill at about 1.5 m which coincides with the effective correlation range chosen for the random fields. A similar range of spatial correlation is obtained in the low infiltration *Case U1* (x-direction). However, in cases of intermediate saturation the correlation in space seems much smaller. For example, in *Case U3* the effective range of correlation is about 0.6 m which is almost three times smaller than the initial spatial correlation chosen for the absolute permeability field. Apparently the infiltration rate not only changes the heterogeneity of the effective permeability field, but also the spatial correlation. In cases of intermediate domain saturation, the flow system becomes more homogeneous **and** features smaller correlation ranges.

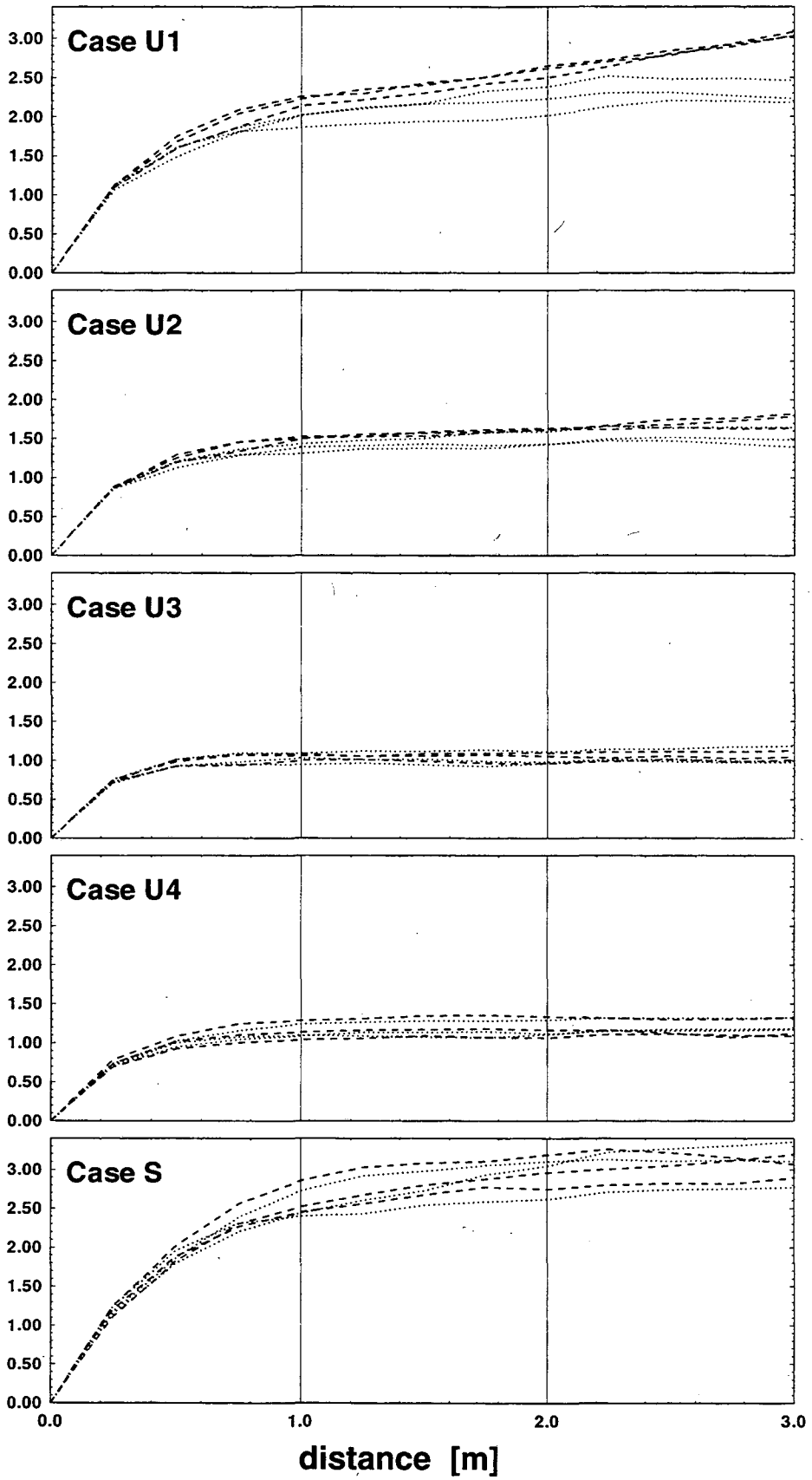

Fig. 16: Semi-variogram of effective permeability, for three different realizations of the random field (dotted line: x-direction, dashed line: z-direction)

3.2 Solute Transport Field

In this section we present results of particle tracking simulations performed for the different infiltration rates. These results are carefully analyzed and studied to obtain (1) a better understanding of the phenomenology of channeling in variably saturated flow fields and (2) a better understanding of the impact of heterogeneity and mean domain saturation on particle arrival times or the dispersion phenomenon. As already mentioned, we consider a steady-state flow situation, and the tracking procedure is performed with steady-state particle velocities.

Particle Tracks

Figures 17, 18, 19, 20 and 21 show particle traces calculated for the different test cases. For the sake of a better visualization, we present only 50 particles which are chosen randomly out of the 300 released at the top boundary of the model area. The number of particles introduced at each location is proportional to the infiltration rate at that point, i.e. we assume that the infiltrated water has a uniform concentration value. We follow the particles through the model area, collect them at the bottom boundary and record the travel time taken by each particle. For each of the five scenarios with different infiltration rates, we present a sequence of three time periods, chosen to be 10 %, 40 % and 100 % of t_{MEAN}, with t_{MEAN} defined as the mean travel time of the fastest 90 % of the 300 particles. The traces of particles that have been transported in these time periods are drawn as black lines. Only one particular realization of the random absolute permeability field is chosen for all these figures; it is the same realization as presented in section 3.1.

The low saturation *Case U1* (in Fig. 17) and the fully saturated *Case S* (in Fig. 21) clearly indicate the existence of solute channeling. Particles (or solutes) travel mainly along preferred flow paths while large parts of the model area are not affected. In both cases we observe three major channeling zones each containing a number of particle traces. These zones would be associated with a high contaminant concentration. The other parts of the model area, which hardly contain any particle traces, can only be contaminated through molecular diffusion processes, and thus would be associated with very low contaminant concentration values. Consequently, field tracer tests have to be designed in a way that the heterogeneity of the solute transport is recorded, for example by performing line measurements rather than highly localized ("point") measurements [*Moreno et al.,* 1990]. As already stated in previous paragraphs, the degree of channeling appears to be similar for *Cases U1* and *S*; however, the locations of the channels are very different.

For infiltration rates higher than that of *Case U1* we observe a different picture. Especially *Case U3* (in Fig. 19) and *Case U4* (in Fig. 20) exhibit widely spread particle paths where channels can hardly be identified. The particles cover almost the entire model area, indicating a fairly homogeneous concentration field.

A comparison of the results for different time intervals within a time sequence indicates that the transport along preferred flow paths can be much faster than the average transport in the entire area. In *Case U1*, for example, some particles have almost reached the bottom boundary of the model area after a time period 0.4 x t_{MEAN}. At the same time, other particles are still close to the input cross section since they are apparently moving in low velocity zones. A similar picture can be observed in *Case S*. Then, with increasing saturation levels as in *Cases U2, U3* and *U4*, the differences between fast and slow flow paths decrease; an almost spread-out solute front is moving through the model area and the channeling effect is much less pronounced.

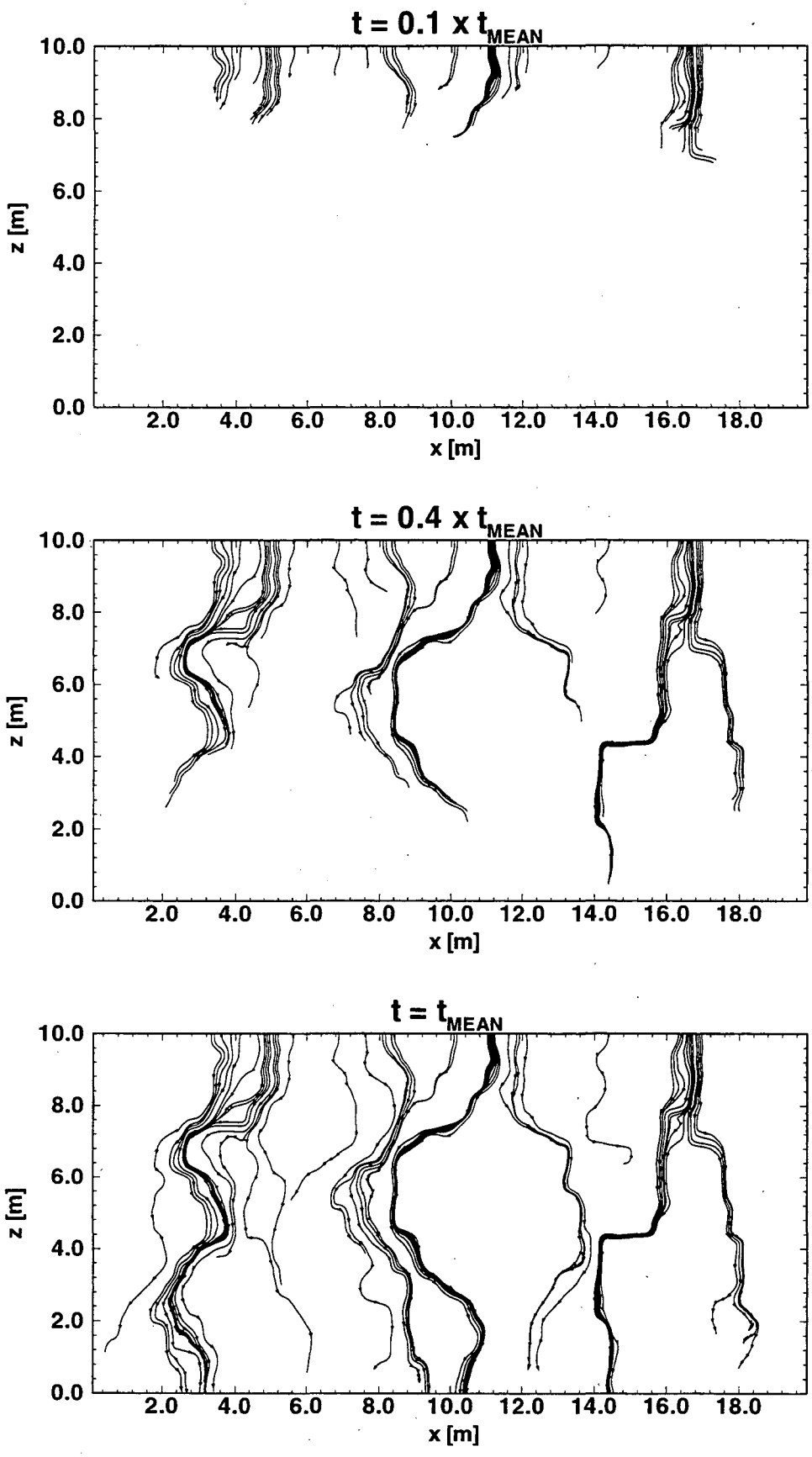

Fig. 17: Particle tracks for *Case U1* (Q_{inf} / Q_{inf}^{sat} = 10^{-5})

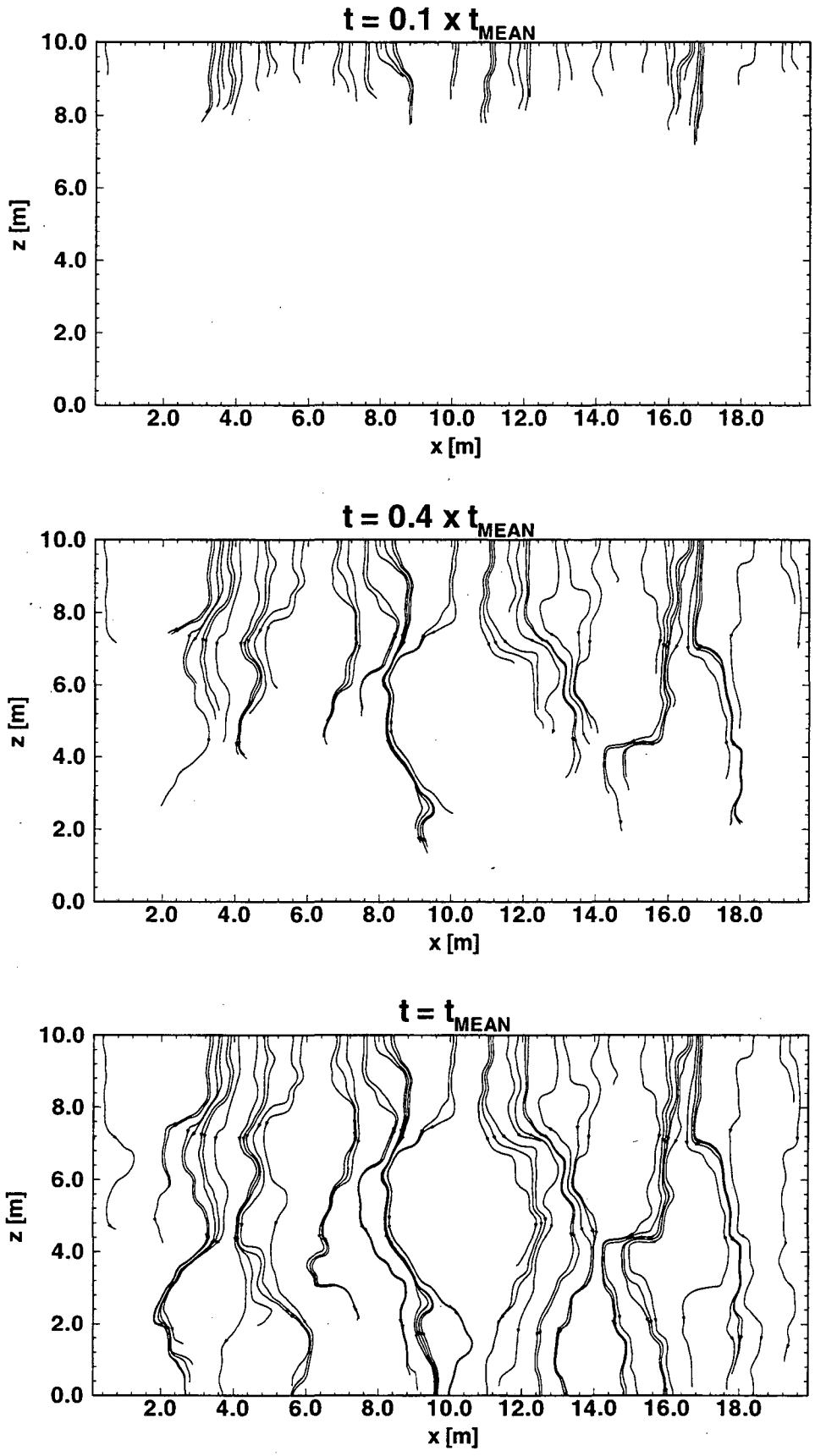

Fig. 18: Particle tracks for *Case U2* (Q_{inf} / Q_{inf}^{sat} = 10^{-3})

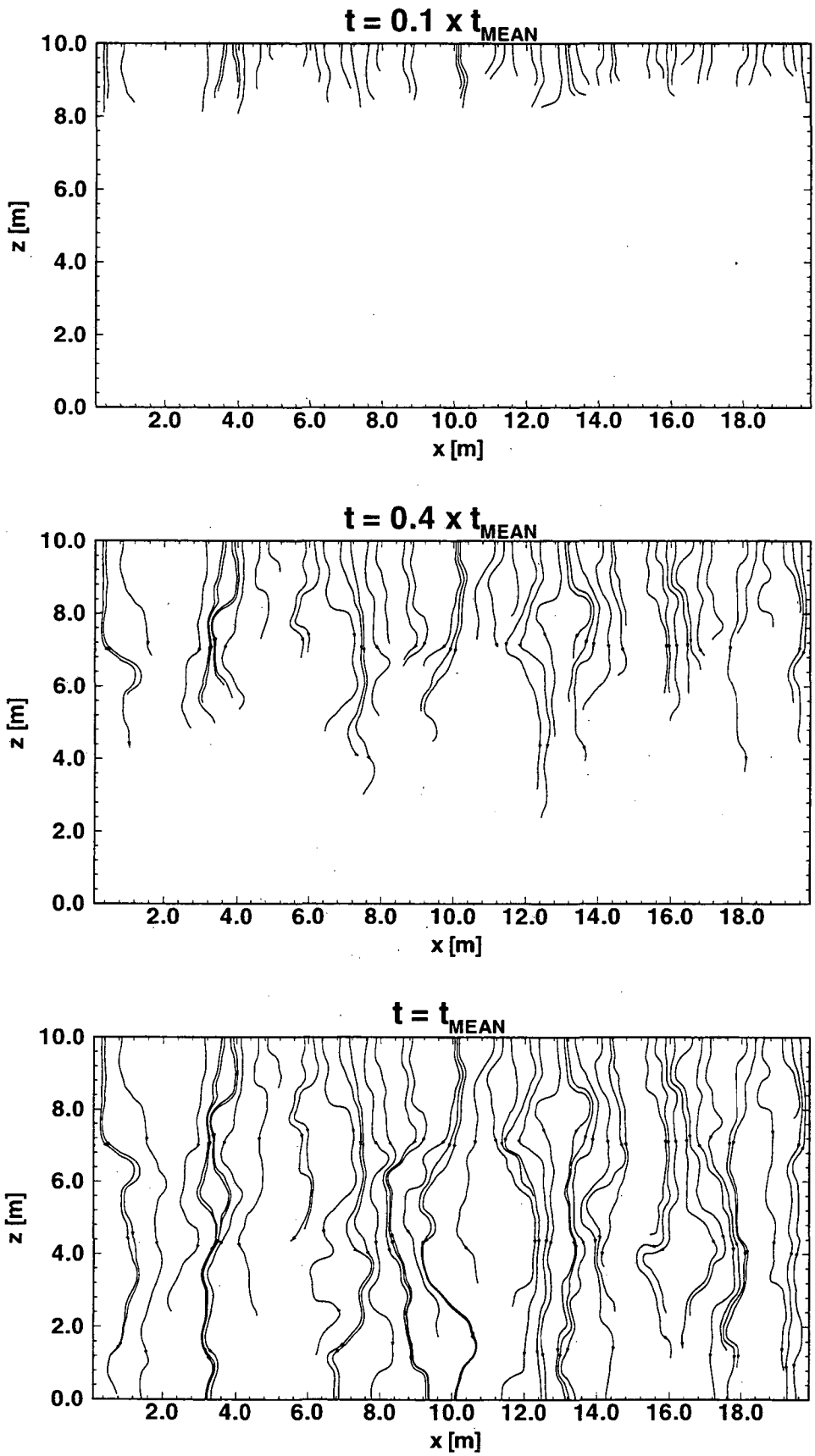

Fig. 19: Particle tracks for *Case U3* (Q_{inf} / Q_{inf}^{sat} = 10^{-2})

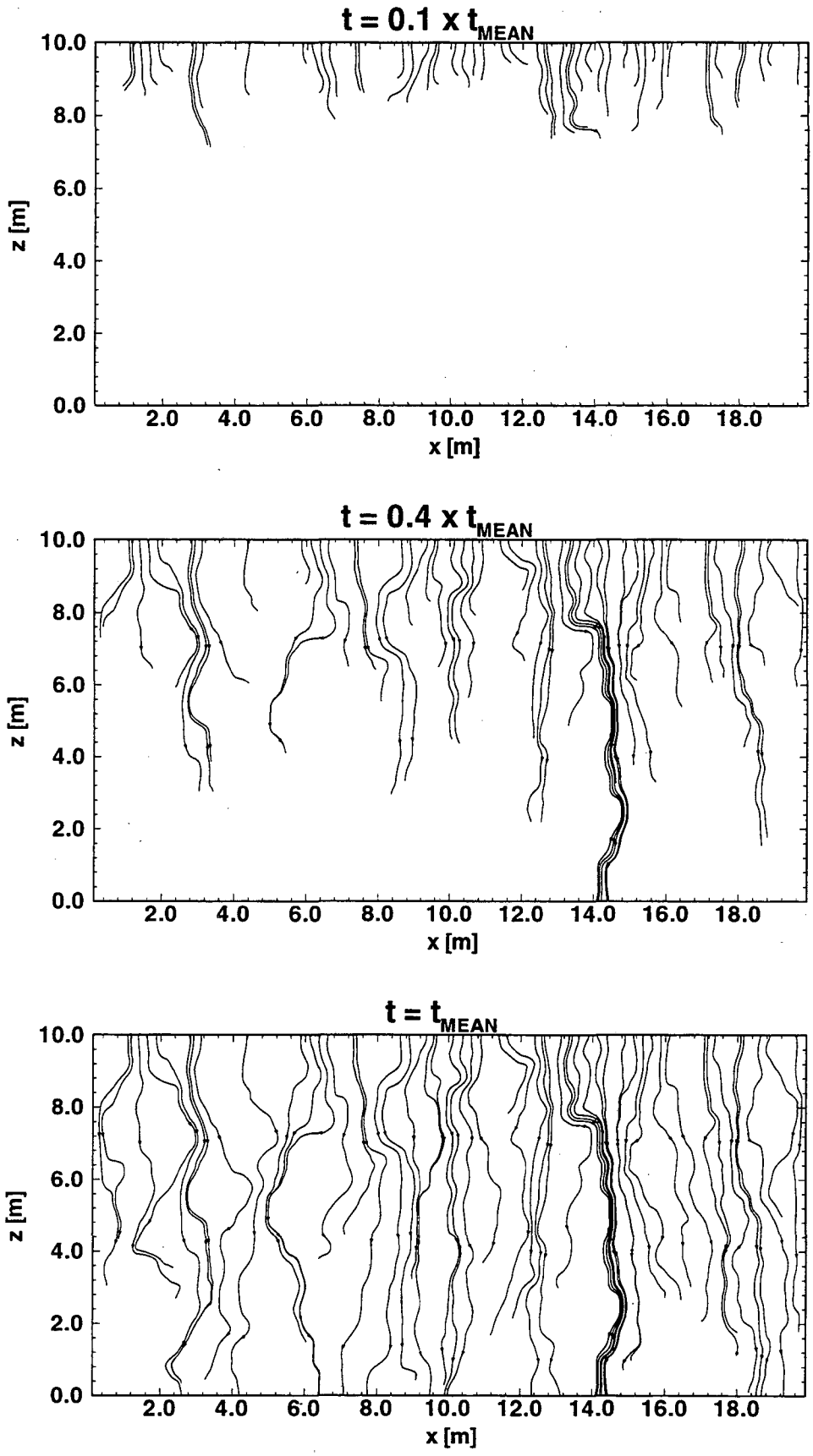

Fig. 20: Particle tracks for *Case U4* ($Q_{inf} / Q_{inf}^{sat} = 10^{-1}$)

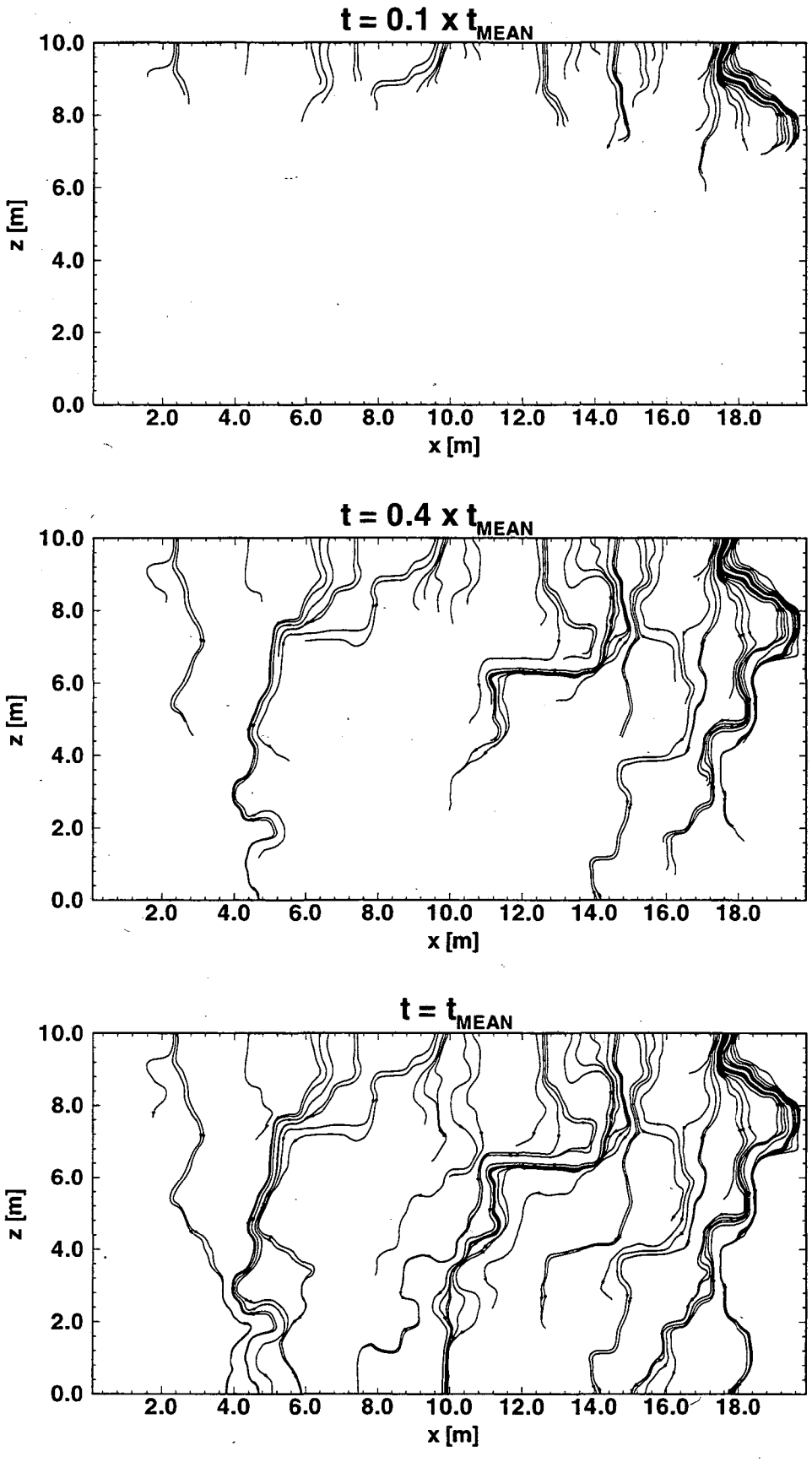

Fig. 21: Particle tracks for *Case S*

These results have some interesting implications for solute transport in heterogeneous fields, in that the location of particle paths changes with the infiltration rate. For example, contaminated soil can be cleaned by imposing large flow rates to dilute the water. However, when the area of concern has been contaminated during a low precipitation period this dilution process can be much less effective than expected because the hydraulic structure of the system reverses completely with larger infiltration rates. As a consequence, in-situ remediation strategies for variably saturated media have to consider the mean domain saturation to avoid failure. Moreover, intentionally modifying the hydraulic structure of flow systems might offer new clean-up possibilities: Low-flux zones which have been contaminated mainly due to diffusion processes may directly be cleaned when converted into high-flux zones by changing the infiltration rate [*Roth*, 1995]. Another implication is related to retardation of radionuclides from a nuclear waste repository in a variably saturated geologic medium. As saturation changes, major flow paths also change, thus making new rock surface areas accessible for chemical reactions and retardation.

Statistics of the Channel Properties

In this section we present the hydraulic properties of the channels and compare them to the hydraulic properties of the entire porous medium. First, we are interested in the correlation between the absolute permeabilities as an intrinsic characteristic of the geologic system and the preferential particle paths obtained for the different mean domain saturations. The absolute permeability values along the particle traces of the 90 % fastest particles are collected and plotted as a frequency distribution (the channel distribution). The mean and the standard deviation of this distribution are calculated and compared to the respective values of the entire flow domain.

Figure 22 shows the frequency distributions obtained for the different test cases. All three realizations of the random permeability field are included. The heavier solid lines give the channel frequency distributions, the dashed lines give the frequency distributions for the entire flow field, as provided by the random field generator. It is obvious from Figure 22 that (1) the absolute permeabilities along channels are different from the properties of the entire flow domain and (2) the absolute permeabilities along channels strongly depend on the degree of saturation. In *Case S* the majority of the absolute permeability values along the channels is much higher than the mean absolute permeability of the entire flow domain. This is reasonable since channels in fully saturated media develop along interconnected zones of high absolute permeabilities. Then, for the cases with smaller infiltration rates, the absolute permeabilities measured along channels decrease significantly; the frequency distributions shift to lower values. This is also reasonable since areas of large absolute permeability drain first with decreasing saturation and do not contribute anymore to the main flow and transport processes. All channel distributions are more narrowly peaked than the distributions of the entire flow field, indicating a smaller heterogeneity along the channels. This exemplifies the fact that channels choose the least resistive paths in the flow field; thus the variation of absolute permeabilities along channels is naturally smaller than the variation in the entire domain.

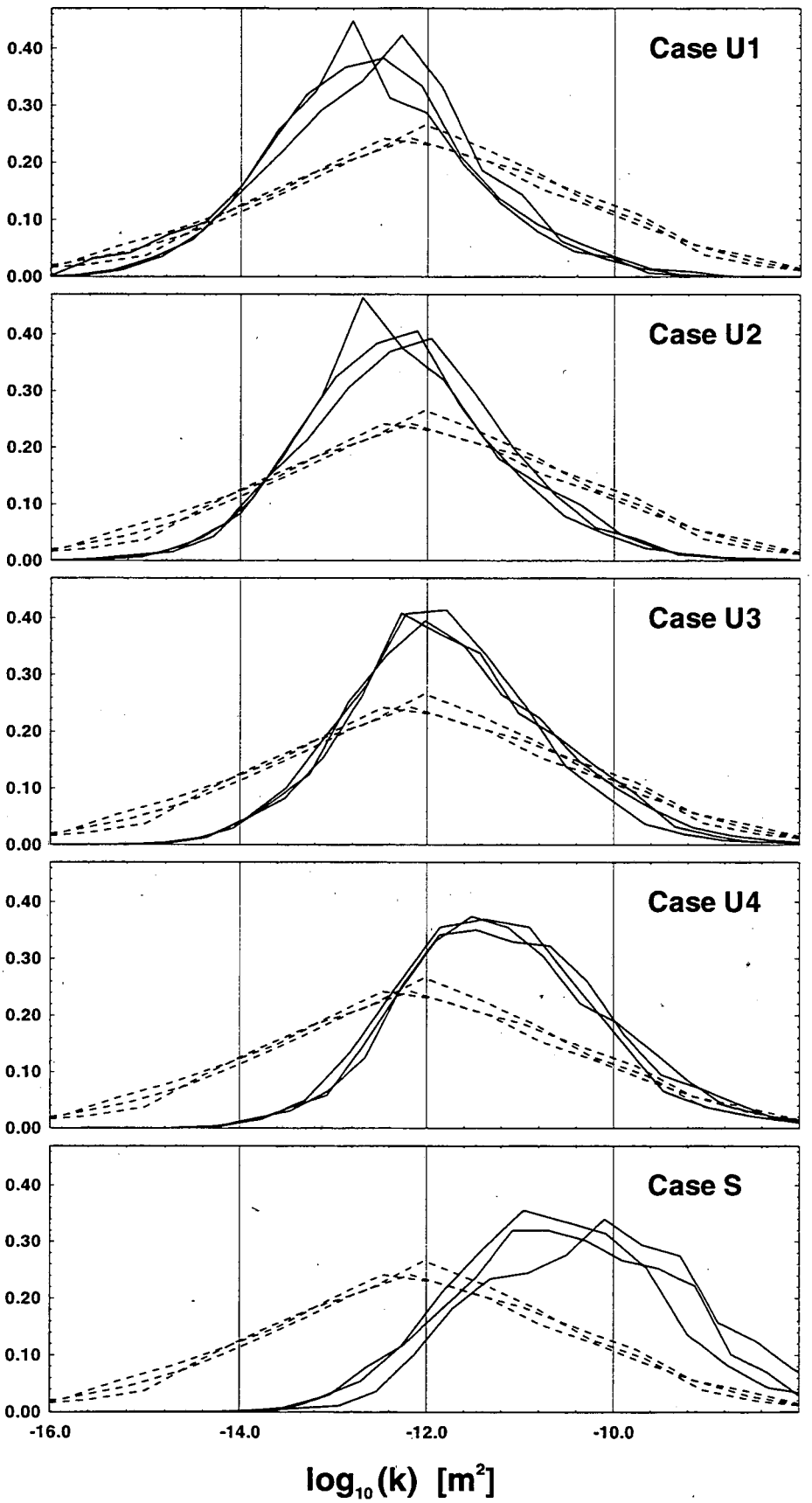

Fig. 22: Frequency distribution of absolute permeability for the channels and the entire flow domain, for three realizations of the heterogeneous field

Figures 23 and 24 provide a summary picture of the absolute permeability distributions by giving the geometric mean and the standard deviation. Again, all realizations are included. The heavier lines with symbols represent the channel properties and the horizontal lines represent the properties of the entire flow domain. Note that the actual mean and standard deviation of the entire flow domain for the three realizations do not exactly coincide with the input values for the random field generator.

Figure 23 shows that for *Cases U3, U4* and *S* the mean absolute permeability of the channels is higher than the mean absolute permeability of the entire flow domain, indicating that in all these cases the maximum values of effective are found in areas of intermediate to high absolute permeabilities. This changes when the mean domain saturation decreases further. For *Cases U1* and *U2* the hydraulic structure of the flow field is completely reversed. Here, the mean absolute permeability along channels is smaller than the mean absolute permeability of the entire flow domain. The least resistive paths are now those along low absolute permeability zones which are associated to small pore sizes and strong capillary suction. Hence, these zones maintain higher saturations than areas of large absolute permeabilities, and eventually their effective permeability values become higher.

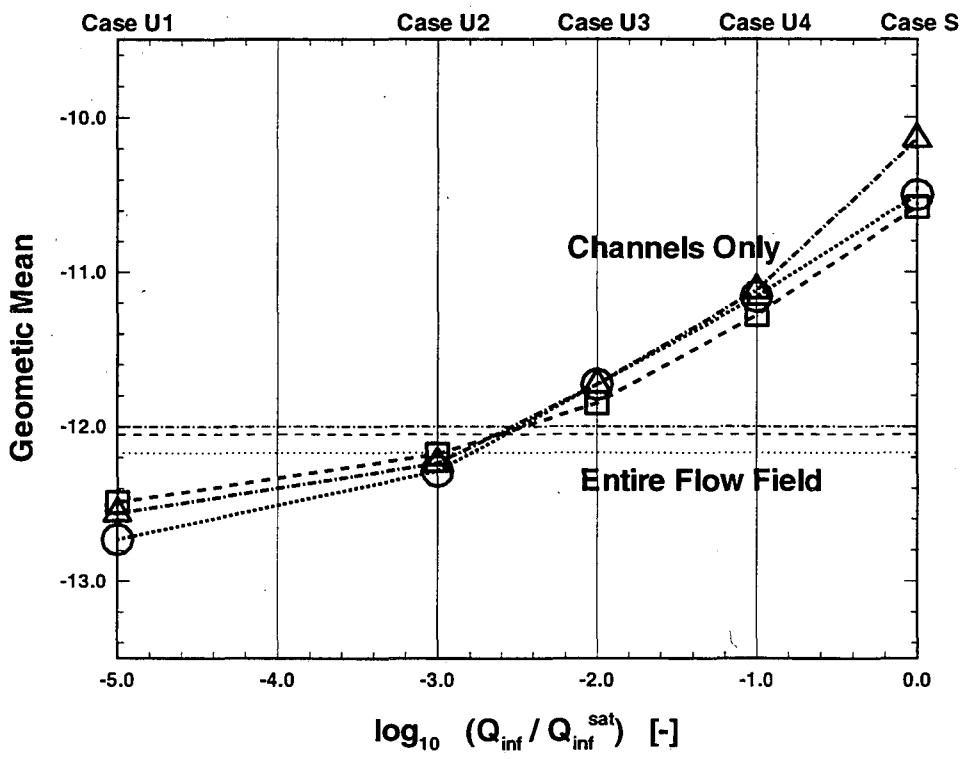

Fig. 23: Mean absolute permeability (in $\log_{10}$ m^2) for the channels and the entire flow domain as a function of the infiltration rate, for three realizations of the heterogeneous field

Figure 24 demonstrates that the channels distributions of absolute permeability have smaller standard deviations than the distributions for the entire flow domain. It is interesting that the channel standard deviations of all cases very similar, despite of the fact that the hydraulic structure of these cases is very different.

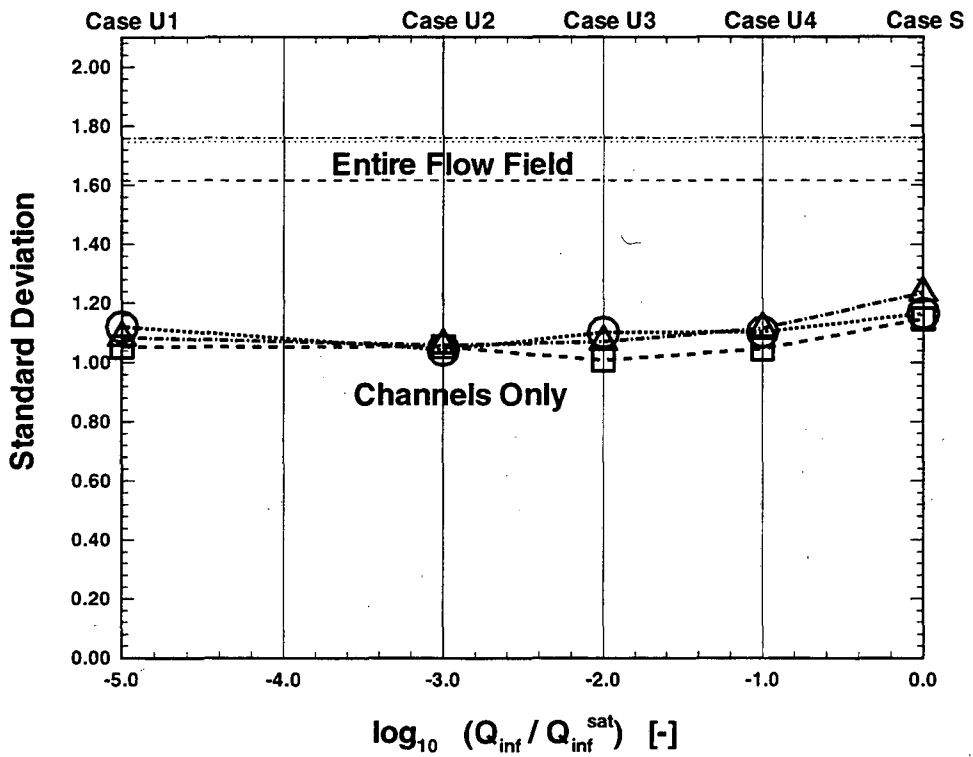

Fig. 24: Standard deviation of absolute permeability (in $\log_{10}$ m^2) for the channels and the entire flow domain as a function of the infiltration rate, for three realizations of the heterogeneous field

Now let us study the effective permeability measured along the particle traces. Under partial saturation the effective permeability distribution defines the flow rate through channels as well as the variation of flow along the channels. In Figure 25 we compare the mean log effective permeability of the channels with the mean log effective permeability of the entire flow field. Remember that for *Case S* the effective permeability is equal to the absolute permeability. It is obvious that (1) channels are more (effectively) permeable than the entire flow domain, and that (2) cases with intermediate saturation exhibit the smallest differences between the channel distribution and the distribution of the entire flow domain. This is consistent with the earlier observation that the degree of channeling is smaller for *Cases U2, U3* or *U4* than that of *Cases U1* and *S*.

Figure 26 presents the standard deviations of the effective permeability distributions for the channels and for the entire flow field, respectively. The latter have previously been presented in Figure 15. While all channel distributions have smaller standard deviations than the global distributions, the statistics of the channels follow the same trend as the statistics of the entire flow domain, i.e. the smallest standard deviations are found in cases of intermediate infiltration rate. The differences between the channel standard deviations and the global standard deviations, however, appear to decrease with increasing mean domain saturation. As a result, the unsaturated cases exhibit a smaller variety of effective permeabilities along the channels than the saturated case. In particular, in *Case U1* we observe the channel standard deviations to be in the range of 0.8, whereas in *Case S* we observe values around 1.2. This is in contrast to the statistics of the entire flow domain, which indicates that the standard deviations in *Case U1* are slightly higher than in *Case S*. Apparently, the statistical properties of the **entire flow domain** may not provide a good estimate for the characteristics of flow and transport **along channels**. This will be further discussed when analyzing the tracer breakthrough in such systems.

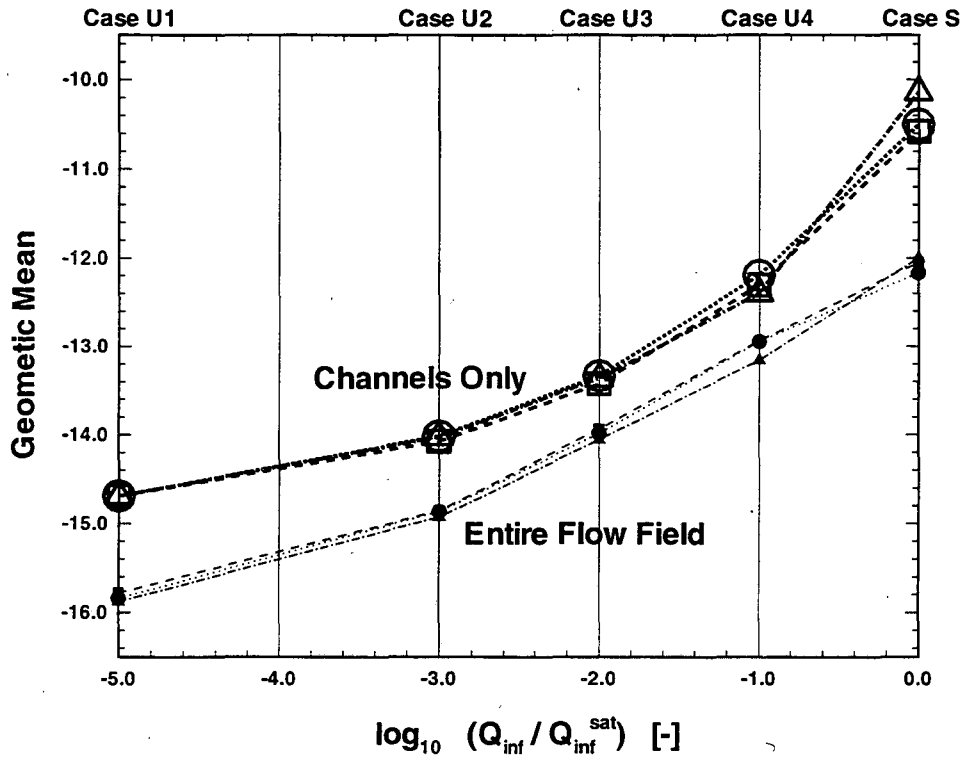

Fig. 25: Mean effective permeability (in $\log_{10}$ m^2) for the channels and the entire flow domain as a function of the infiltration rate, for three realizations of the heterogeneous field

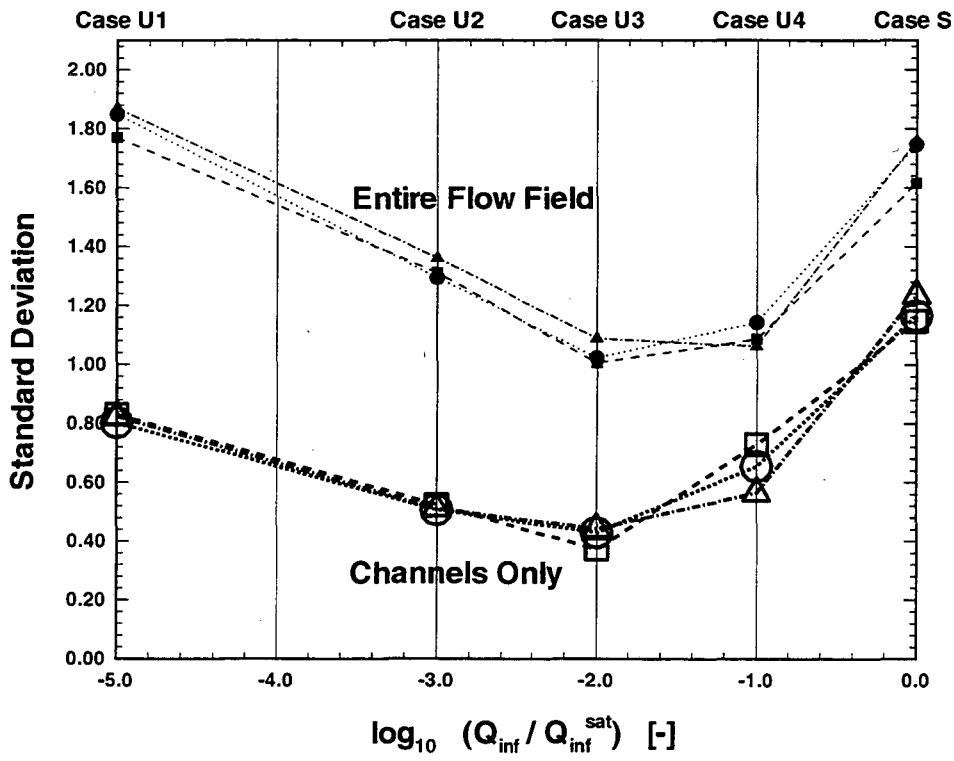

Fig. 26: Standard deviation of effective permeability (in $\log_{10}$ m^2) for the channels and the entire flow domain as a function of the infiltration rate, for three realizations of the heterogeneous field

Let us finally study the statistics of the water saturation, presented in Figure 27 (arithmetic mean) and Figure 28 (standard deviation). The mean saturation values show that channels tend to follow the higher saturated zones of the flow field. The lower is the infiltration rate, the larger is the difference between the mean saturation of the channels and the mean saturation of the entire domain. The channel saturations are more homogeneous than the saturation values in the entire flow field, indicated by smaller standard deviations. Naturally, *Case S* is exceptional because of its uniform saturation value of 1.0, resulting in a zero standard deviation.

A common characteristic of all figures presented in this section is the fact that the three realizations exhibit very similar statistical results for the channel properties, with only minor differences in mean values and standard deviations. Essentially, these minor differences in the channel statistics are in the same range as the differences in the statistics of the entire flow field for the three realizations. Thus, we may conclude that they mainly originate from the random procedure to generate the absolute permeability fields.

The similarity of the three realizations with regard to the channel statistics is interesting when considering that the ***actual locations*** of channels can be totally different for the realizations of a particular test case. Only the ***degree*** of channeling is similar. Thus, the statistical properties of the channels are independent of the specific locations and geometry, and may be an intrinsic characteristic of the heterogeneous medium and the degree of saturation. Then, it seems possible to characterize the flow and transport processes in a variably saturated medium by providing the statistical properties of the channel distribution only [*Chesnut*, 1992 and 1994].

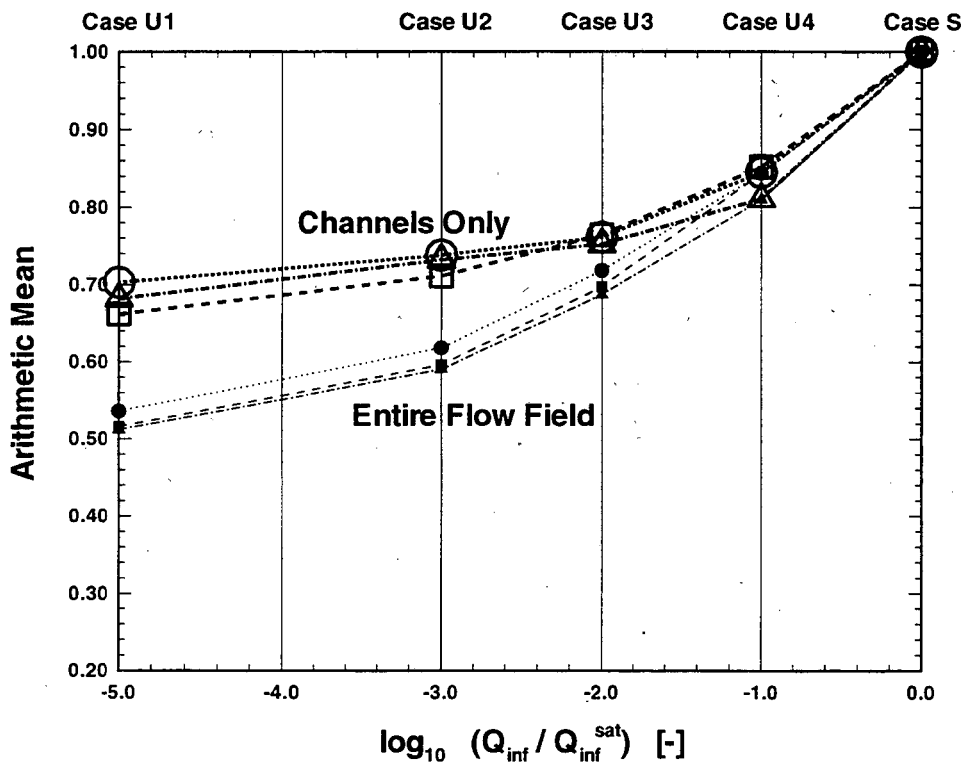

Fig. 27: Mean saturation for the channels and the entire flow domain as a function of the infiltration rate, for three realizations of the heterogeneous field

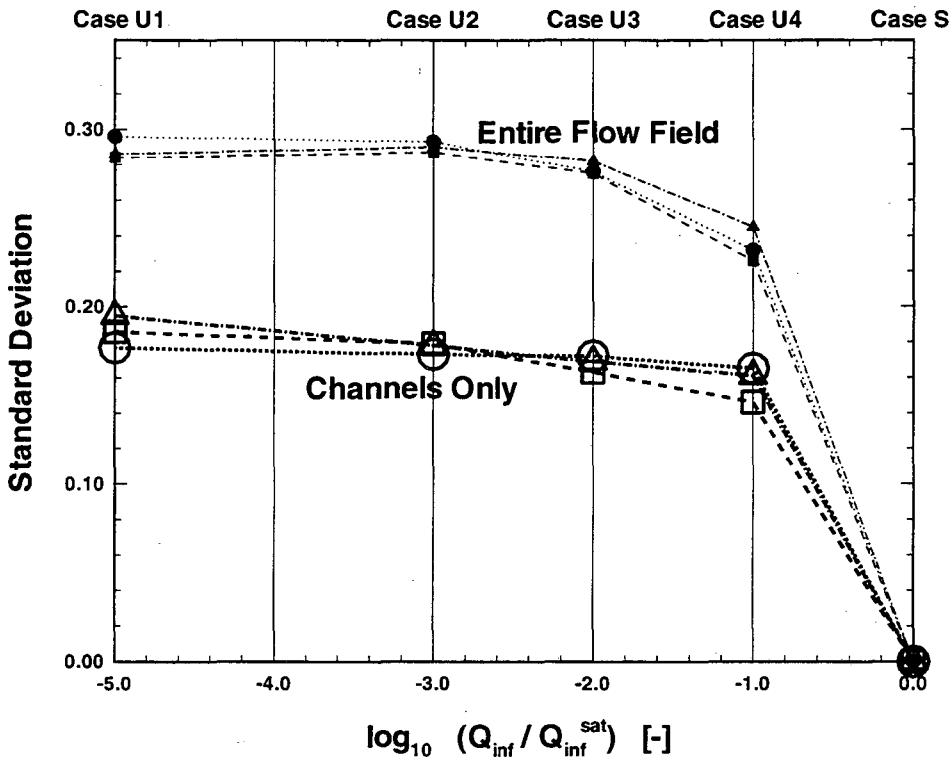

Fig. 28: Standard deviation of saturation for the channels and the entire flow domain as a function of the infiltration rate, for three realizations of the heterogeneous field

Tracer Breakthrough Curves

In this section we study the characteristics of solute transport in terms of tracer breakthrough curves, by collecting the fastest 90 % of the particles, calculating their travel times from the top to the bottom boundary and grouping them into specified intervals of arrival times. The results represent tracer mass versus arrival time curves from a pulse tracer injection test. Figure 29 shows the simulated curves for all cases and three realizations of the random field. The dashed curves correspond to the particular realization shown in Figures 6-13 and 17-21. The travel time on the horizontal axis is presented as a dimensionless variable, with the actual travel time divided by the mean travel time of all particles. The numbers on the vertical axis denote the relative number of particles arriving at the bottom boundary within a certain time interval; i.e. the actual number of particles is divided by the total number of particles. Note that in Figures 17-21 only 50 particle traces are presented while the curves in Figure 29 are calculated with 300 particles. This gives rise to minor discrepancies.

Let us first discuss some results of a previous study on solute transport in ***saturated*** media of variable heterogeneity [*Moreno & Tsang*, 1994]. It has been found in this study that for small standard deviations of absolute permeability most particles travel with the mean particle velocity; i.e. tracer breakthrough curves would present a peak at $t/t_{MEAN} = 1.0$, with values around the peak value spreading out as the standard deviation increases. However, for very large standard deviations, a new peak at much earlier times emerges, indicating the strong effect of channeling in very heterogeneous media. Particles traveling in channels are transported many times faster than particles traveling in homogeneous media. *Moreno & Tsang* refer to this as the "fast channeling effect". At the same time, some particles are traveling at least part of their way in low absolute permeability zones, and then their travel time is much larger than t_{MEAN}. This results in the typi-

cal long tail of the breakthrough curves. For intermediate standard deviations an interesting transition is observed: The tracer breakthrough is wide and diffused; a distinct peak value can hardly be identified.

As a matter of fact, all of the above presented characteristics can be found in the tracer breakthrough curves shown in Figure 29. However, in our study the absolute permeability fields have a uniform degree of heterogeneity with a large standard deviation of 1.737 (in $\log_{10}$ m^2) which, according to the findings of *Moreno & Tsang*, gives rise to strong channeling effects. Thus, the differences between the test cases are **not** originating from different degrees of heterogeneity in the absolute permeability field, but only from the different degrees of saturation.

In *Cases U1* and *S* we obtain tracer breakthrough curves which are typical for solute transport in heterogeneous flow fields with strong channeling effects. The peak travel times are very short, meaning that a significant part of the solute is transported many times faster than the mean time for the bulk of the fluid. Some of the curves exhibit two or three early peaks, indicating that particles are transported in two or three fast channels. The tracer breakthrough curves would be smoother for larger model areas when more channels were included.

For cases with an intermediate degree of saturation the tracer breakthrough curves are very different. In particular, *Case U3* represents the typical curve of a homogeneous porous medium with low dispersion. The peak travel time almost corresponds to t_{MEAN}, and the differences between first and last arrival are smaller. Also, the shape of the curves is smoother than in the early peak cases; apparently the solute is now transported by many near-vertical channels.

Case U4 exhibits very wide and dispersed tracer breakthrough curves, with a significant number of particles arriving at both early and late times. Also, the peak values are smaller than in the other cases. According to *Moreno & Tsang* this behavior is typical for intermediate degrees of heterogeneity. Note that in Figure 13 we observed a similar degree of channeling for *Case U3* and Case *U4*. Moreover, the standard deviations of effective permeabilities in the entire flow domain were about in the same range for both cases (see Fig. 15). Thus we would expect the tracer breakthrough curves of these two cases to be similar as well; however, there are very obvious differences. Then, since the degree of channeling is the same, we may conclude that the flow ***along*** the channels is more heterogeneous in *Case U4* than in *Case U3*. Indeed Figure 26 shows that the standard deviations of effective permeabilities along the channels are higher in *Case U4*. We assume at this stage that this behavior is caused by the structure of the saturation field: *Case U4* represents a transition scenario between predominantly unsaturated flow and fully saturated flow; thus it features characteristics of both types of flow. However, this aspect needs further study and consideration.

Our results have some implications with regard to the analysis of field tracer tests in variably saturated media. It is apparent that the characteristics of solute transport are strongly dependent on the saturation of the soil. Thus, the dispersivities derived for a certain level of saturation may be completely meaningless for a case of a different level of saturation. In particular, the transport behavior under predominantly unsaturated conditions cannot be simply estimated from tracer breakthrough curves of predominantly saturated flow, and vice versa. A thorough interpretation of field tracer tests is thus not possible without taking the actual saturation of the flow field into account.

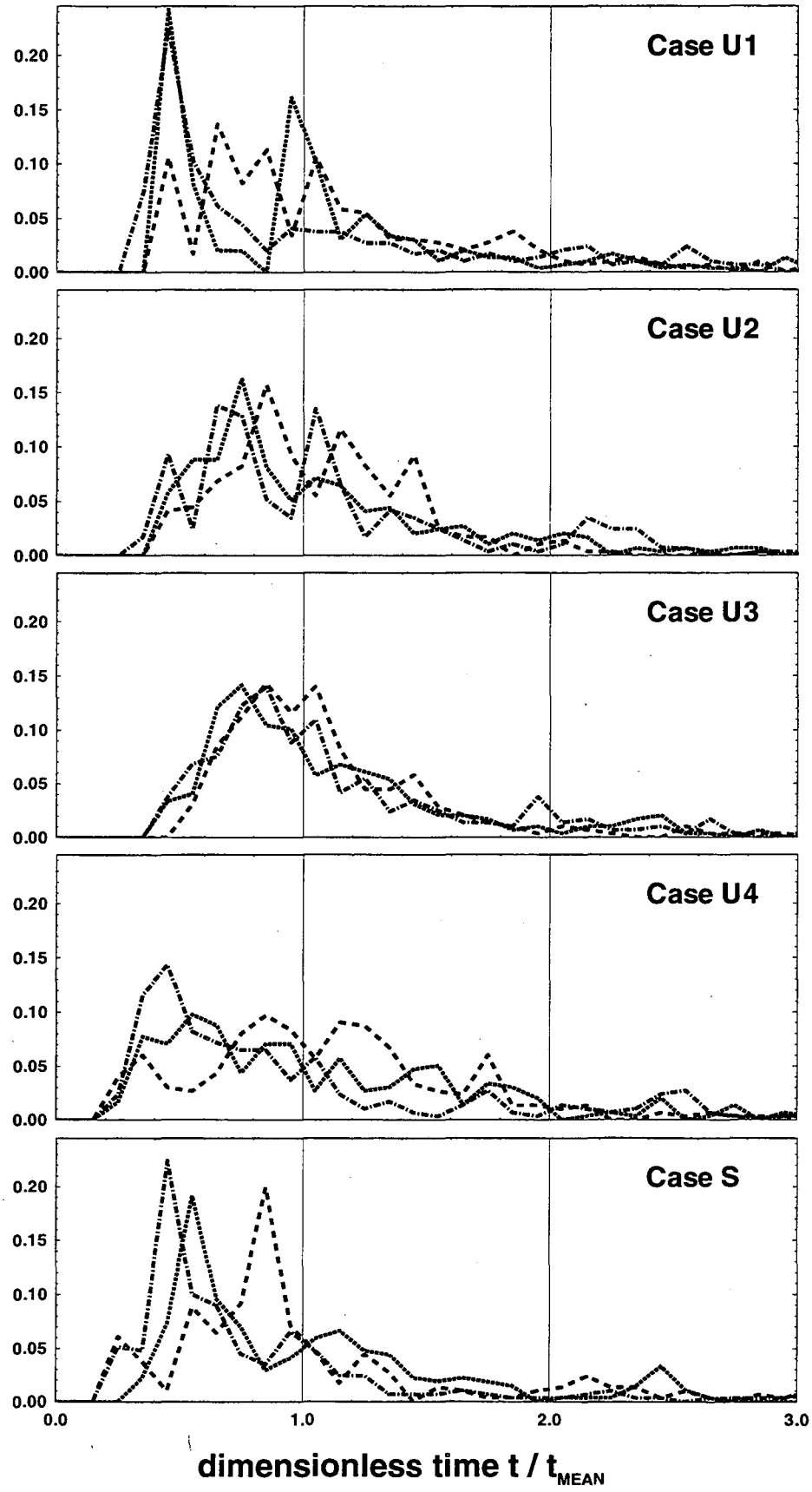

Fig. 29: Tracer breakthrough curves for a pulse injection, for three realizations of the heterogeneous field

Sahimi et al. [1986a and 1986b] used a percolation approach to study tracer dispersion in two-phase flow systems with random heterogeneity. Their results indicate that the heterogeneity of the flow system **constantly** increases as the mean saturation level decreases; i.e. a "smoothing" effect within intermediate saturation ranges, as found in our study, is **not** obtained. These differences may be due to the different conceptual models used. While our study (and the study of *Roth* [1995] which gives similar results) follows the continuum concept of unsaturated flow, and describes the porous medium with effective continuum parameters such as saturation and relative permeability, Sahimi et al. use a pore scale model which simulates the soil as a network of orthogonal stream tubes with random radii. The capillary pressure value corresponding to the pore radius of a tube determines if it is occupied or not by the wetting phase. Thus, with decreasing saturation, more and more tubes drain and become completely inactive for flow. The remaining network of conductive tubes becomes very sparse and tortuous, and finally approaches a state where only isolated clusters of connected tubes exist (percolation threshold). This procedure gives rise to a strong increase in dispersivity with decreasing saturation. With continuum models, on the other hand, the entire model area is always conductive, although the conductivity may be almost negligible for low saturations. Thus the connectivity of flow paths is not an issue. Another reason for the differences might be that Sahimi et al. use non-correlated distributions of tube radii. As a consequence, the probability of tubes with similar radii forming long conductive channels is rather small. On the other hand, we use a correlated heterogeneous field generated by recently developed methods.

3.3 Dependence of Results on Type of Lower Boundary Condition

Up to now it was assumed that the lower boundary of the model area coincides with the groundwater table, i.e. $S = 1.0$ and $P_{cap} = 0.0$ along this boundary. This conceptual model represents shallow groundwater systems where the area of interest is adjacent to the saturated zone. However, in particular cases one might be interested in deep geologic systems with a very extended vadose zone. Then, the groundwater level might be much lower than the area of interest, and does not affect the hydraulic variables in the model area. To study such cases, we perform simulation runs with a different lower boundary condition; i.e. for each saturation scenario we impose the same capillary pressure value along the lower boundary as that chosen for the upper boundary. Then the saturation and capillary pressure values are macroscopically uniform in the model area, and such is the gradient of hydraulic head. Figures 30, 31 and 32 show vertically distributions of saturation, capillary suction and hydraulic head, calculated for the new set of boundary conditions and presented for one particular realization of the random field. All values are averaged over the width of the model area (compare to Fig. 8, 9 and 10 for the original set of boundary conditions).

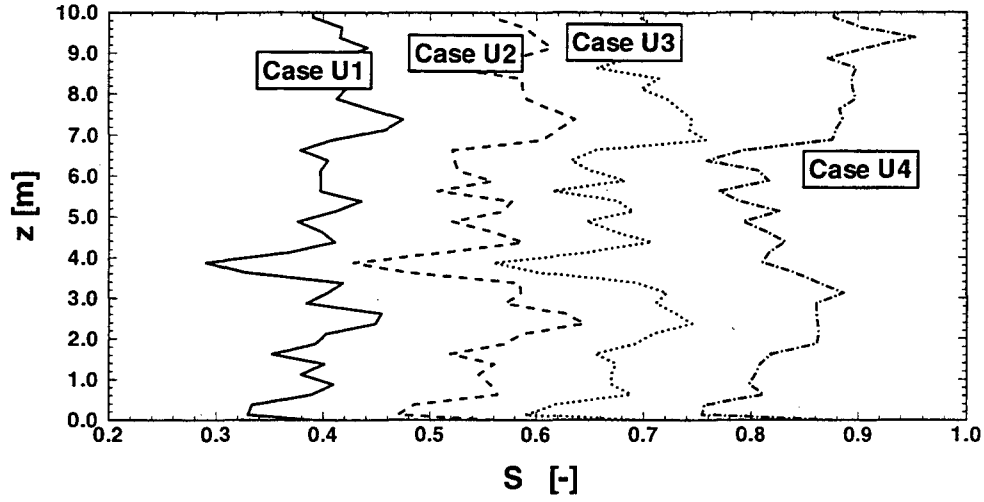

Fig. 30: Vertical saturation profile, values averaged over width of model area

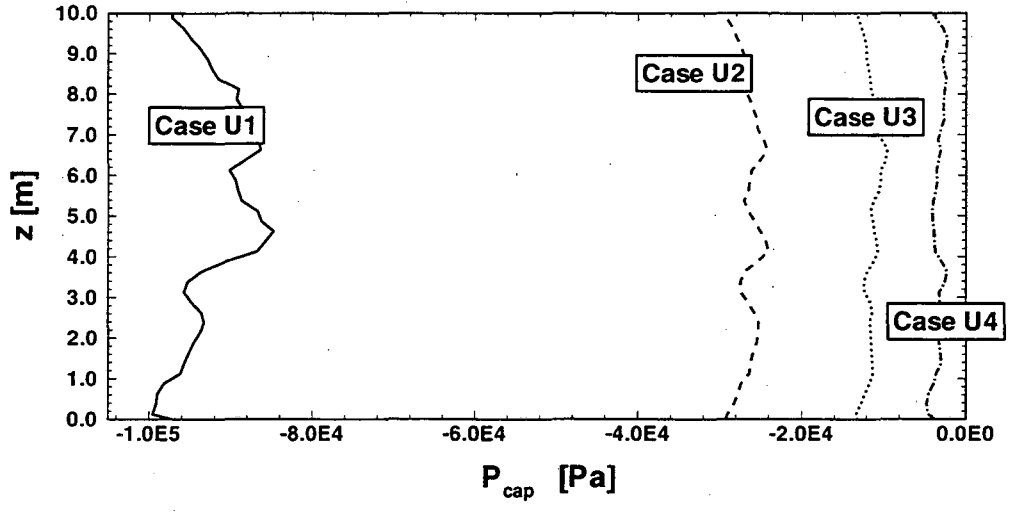

Fig. 31: Vertical capillary pressure profile, values averaged over width of model area

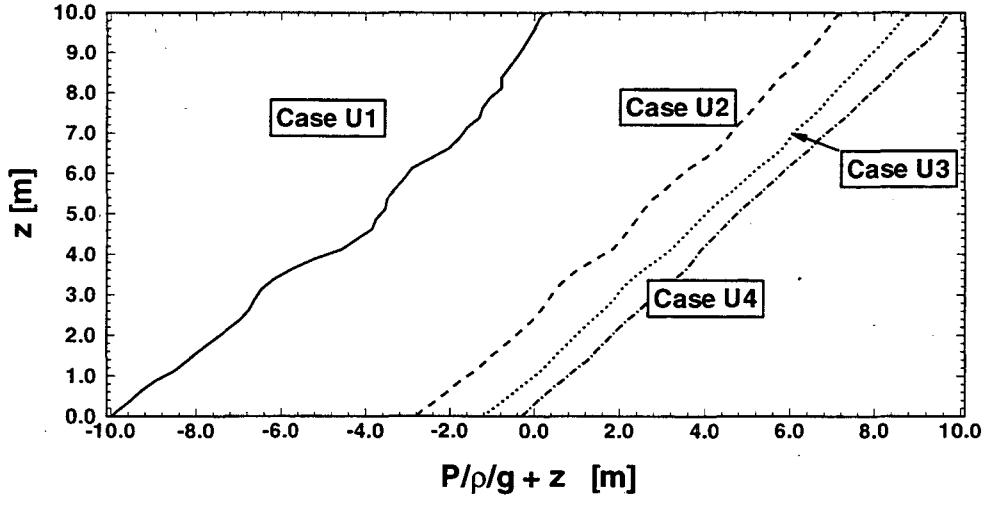

Fig. 32: Vertical profile of hydraulic head, values averaged over width of model area

Our simulation results show that the general findings of the previous sections hold for the new boundary condition as well. Naturally, the main differences between the two types of boundary condition occur for *Case U1* which is strongly influenced by the "groundwater table" at the bottom of the model area. However, even in *Case U1* the characteristics of flow and solute channeling are essentially similar for the two different boundary conditions. As an example for the results of the new simulation runs, Figure 33 depicts the standard deviations of the effective permeability distribution for the channels and the entire porous medium. The solid lines give the results obtained with the new capillary pressure boundary condition, and the dashed lines show the results calculated with the original lower "groundwater table" boundary condition, as presented in Figure 26.

It is obvious from Figure 33 that the most prominent features of the effective permeability distribution are preserved; e.g. the reduction of the effect of heterogeneity for intermediate saturation levels, and the fact that the heterogeneity of flow **along** the channels is higher for flow fields with almost full saturation. The latter phenomenon is even more pronounced with the new boundary condition; apparently because the flow field is not influenced by a certain trend of hydraulic properties in vertical direction.

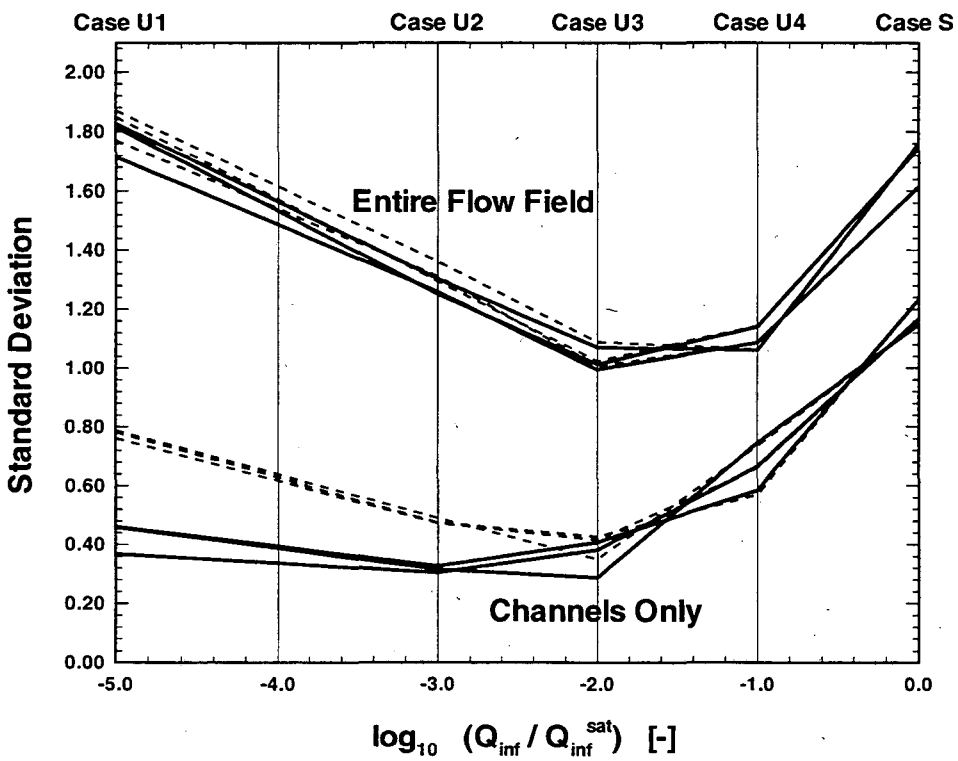

Fig. 33: Standard deviation of effective permeability (in $\log_{10}$ m^2) for the channels and the entire flow domain as a function of the infiltration rate, for three realizations of the heterogeneous field. The solid lines denote the new lower boundary condition, the dashed lines denote the original lower boundary condition.

3.4 Implications for Field Observations

The existence of flow and solute channeling in heterogeneous, variably saturated media is consistent with a number of experimental findings, such as the high spatial variability in solute concentrations found in some soils [e.g. *Schulin et al.*, 1987; *Flury et al.*, 1994], or the very slow dilution of salts from saline soils [*Thomas & Phillips*, 1979]. A detailed discussion of different experimental studies is given in *Roth* [1995]. However, one of the main conclusions of this study, the dependence of the grade of channeling (and the respective grade of heterogeneity in flow and transport) on the mean domain saturation, has to our knowledge not yet been demonstrated in laboratory or field experiments. *Schulin et al.* [1987] observed significant differences in the spreading pattern of two almost ideal tracers, bromide and chloride, which were applied in different seasons of the year. These differences might partially be caused by the changing flow structure with changing mean domain saturation.

The results of the present investigation point out a new perspective of understanding data obtained in experimental studies. Thus it will be very useful to reanalyze the field observations of transport in unsaturated media keeping in mind the saturation dependence of the flow structure. Moreover, new experiments should be performed, with the focus on the characteristics of flow and transport while different infiltration rates are applied.

The observed dependence of the flow and transport behavior on the mean domain saturation requires a very careful design and interpretation of field tracer tests, in particular in zones with periodic fluctuations of the groundwater table, or in areas with significant differences between dry and wet seasons. Changes in the mean domain saturation might completely reverse the flow structure, they influence the spatial correlation of permeabilities, and they significantly affect the heterogeneity of the flow field, the degree of solute channeling, and the location of channels. As a consequence, dispersivities derived from tracer tests under one set of conditions may be meaningless for another set of conditions. Another aspect is that in-situ remediation strategies have to be designed under consideration of this saturation dependence to avoid failure. As saturation changes, major flow paths also change, and large areas of the flow domain might be less accessible for dilution processes than expected. On the other hand, the possibility of modifying the structure of flow paths by intentionally changing the infiltration rate might offer a new perspective for the clean-up of soils: Low-flux zones which have predominantly been contaminated through diffusion processes may be accessed directly under a different set of conditions. This aspect deserves further attention in future studies.

4 Summary and Conclusions

Numerical simulations have been performed to study flow and solute channeling in a two-dimensional vertical cross-section of a strongly heterogeneous porous medium. Different saturation scenarios were applied varying from fully saturated conditions to highly unsaturated conditions, reflecting different infiltration rates into the flow domain. Three realizations of random absolute permeability fields were generated in our study. The simulation was done with the multi-component, multi-phase simulator TOUGH2 developed at the Berkeley Laboratory. Since we assumed a steady-state flow field we did not address the transient phenomenon of flow fingering at the interface between two phases, which is a different subject of research, studied by a number of other authors.

It was found that the degree of channeling, the location of channels and the hydraulic properties along channels are very much dependent on the mean domain saturation. Strong channeling effects were obtained in both fully saturated and in low saturation cases. However, while with fully saturated conditions channels develop along zones of high absolute permeabilities, in the case of low saturation we find channels only in zones of low absolute permeabilities. Within intermediate saturation ranges, channeling effects are less significant and the system exhibits a more homogeneous flow pattern. Here, the strong heterogeneities in the flow field are dampened, and the standard deviation of the effective permeabilities drops significantly compared to the standard deviation of the absolute permeabilities. Also the spatial correlation changes; the correlation length of the effective permeability field is much smaller in cases of intermediate saturation than in the other cases.

Generally, the mean saturation and mean effective permeability along channels were found to be larger than the respective values for the entire domain. At the same time, the variability of these variables was much smaller when measured along the channels. The specific location and geometry of channels appeared to be very different from realization to realization. However, we found that the hydraulic properties of the channels were independent of the particular realization, provided that the same saturation scenario was considered. Thus, it seems possible to describe flow processes in a variably saturated medium by providing the statistical properties of the channel distribution only.

The characteristics of solute transport in such systems essentially reflect the degree of channeling. In cases when flow channeling is less evident we observed much smaller dispersion effects than in cases with strong channeling phenomena. However, some discrepancies from this general trend were found for cases with predominantly saturated flow. Here, the breakthrough curves were more diffused than the curves obtained for the unsaturated cases, even when a similar degree of channeling and a similar degree of heterogeneity in effective permeability was observed. Apparently, this is originated in the fact that the heterogeneity of flow ***along*** the channels is higher for flow fields with almost full saturation. Thus, the variability of hydraulic parameters in the entire flow domain does not necessarily reflect the dispersive behavior in variably saturated media. Additional information is needed, e.g. the degree of saturation or the variability of the channel properties. This aspect needs further attention in future studies.

The saturation dependence of flow and transport characteristics in variably saturated media has important implications, ranging from the design and interpretation of field experiments to the in-situ remediation of contaminated soils.

Acknowledgment

This work was jointly supported by a NATO-Postdoctoral Fellowship, provided by the German Academic Exchange Organization (DAAD), and by a Feodor-Lynen-Postdoctoral Fellowship, provided by the Humboldt-Foundation, given to the first author. It was also partially supported by the Power Reactor and Nuclear Fuel Development Corporation (PNC), Tokyo, Japan, through the U.S. Department of Energy Contract Number DE-AC03-76SF00098. Review and comments of K. Pruess, Y. Tsang and J. Wang from the Berkeley Laboratory are gratefully acknowledged. We are particularly grateful to K. Pruess and S. Finsterle for making the code TOUGH2 available to the authors, and providing guidance in the use of this code.

References

Chesnut, D.A., Characterizing the altered zone at Yucca Mountain: The beginning of a testing strategy, Proceedings of the Third Annual International High-Level Radioactive Waste Management Conference at Las Vegas, NV., 1026-1039, 1992.

Chesnut, D.A., Dispersivity in heterogeneous permeable media, Proceedings of the Fifth Annual International High-Level Radioactive Waste Management Conference at Las Vegas, NV., 1822-1841, 1994.

Davies, P.B., Evaluation of the role of threshold pressure in controlling flow of waste-generated gas into bedded salt at the waste isolation plant, Sandia National Laboratories report SAND90-3246, Albuquerque, NM, 1991.

Faybishenko, B., Hydraulic behavior of quasi-saturated soils in the presence of entrapped air: Laboratory experiments, *Water Resour. Res.*, 31, 2421-2435, 1995.

Finsterle, S., G.J. Moridis, K. Pruess, A TOUGH2 equation-of-state module for the simulation of two-phase flow of air, water and a miscible gelling liquid, Lawrence Berkeley Laboratory report LBL-36086, Berkeley, CA, 1994.

Flury, M., H. Flühler, W.A. Jury, J. Leuenberger, Susceptibility of soils to preferential flow of water: A field study, *Water Resour. Res.*, 30, 1945-1954, 1994.

Hills, R.G., P.J. Wierenga, D.B. Hudson, M.R. Kirkland, The second Las Cruces trench experiment: Experimental results and two-dimensional flow predictions, *Water Resour. Res.*, 27, 2707-2718, 1991.

Hills, R.G., P.J. Wierenga, Model validation at Las Cruces trench site, Nuclear Regulatory Commission report NUREG/CR-5716, Washington D.C., 1991.

Leverett, M.C. (1941), Capillary behavior in porous solids, *AIME Trans.*, Vol. 142, 1941.

Moreno, L., Y.W. Tsang, C.F. Tsang, F. Hale, I. Neretnieks, Flow and transport in a single fracture: A stochastic model and its relation with field observations, *Water Resour. Res.*, 24, 2033-2048, 1988.

Moreno, L., C.F. Tsang, Y.W. Tsang, I. Neretnieks, Some anomalous features of flow and solute transport arising from fracture aperture variability, *Water Resour. Res.*, 26, 2377-2391, 1990.

Moreno, L.; C.F. Tsang, Multiple peak response to tracer injection tests in single fractures: A numerical study, *Water Resour. Res.*, 27, pp. 2143-2150, 1991.

Moreno, L., C.F. Tsang, Flow channeling in strongly heterogeneous porous media: A numerical study, *Water Resour. Res.*, 30, 1421-1430, 1994.

Moridis, G., K. Pruess, Flow and transport simulations using T2CG1, a package of conjugate gradient solvers for the TOUGH2 family of codes, Lawrence Berkeley Laboratory report LBL-36235, Berkeley, CA, 1995.

Mualem, Y., A new model for predicting the hydraulic conductivity of unsaturated porous media, *Water Resour. Res.*, 12, 513-522, 1978.

Oldenburg, C.M., K. Pruess, On numerical modeling of capillary barriers, *Water Resour. Res.*, 29, 1045-1056, 1993.

Pruess, K., TOUGH user's guide, Lawrence Berkeley Laboratory report LBL-20700, Berkeley, CA, 1987.

Pruess, K., TOUGH2 - A general-purpose numerical simulator for multiphase fluid and heat flow, Lawrence Berkeley Laboratory report LBL-29400, Berkeley, CA, 1991.

Schulin, R., M.T. van Genuchten, H. Flühler, P. Ferlin, An experimental study of solute transport in a stony field soil, *Water Resour. Res.*, 23, 1785-1794, 1987.

Sahimi, M., B.D Hughes, L.E. Scriven, H.T. Davis, Dispersion in flow through porous media - I. One-Phase Flow, *Chem. Eng. Sci.*, 41, 2103-2122, 1986a.

Sahimi, M., A. Heiba, H.T. Davis, L.E. Scriven, Dispersion in flow through porous media - II. Two-Phase Flow, *Chem. Eng. Sci.*, 41, 2123-2136, 1986b.

Thomas, G.W., R.E. Phillips, Consequences of water movement in macropores, *J. Environ. Qual.*, 8, 149-152, 1979.

Tsang, Y.W., C.F. Tsang, Channel model of flow through fractured media, *Water Resour. Res.*, 23 , 467-479, 1987.

Tsang, Y.W., C.F. Tsang, Flow channeling in a single fracture as a two-dimensional strongly heterogeneous porous medium, *Water Resour. Res.*, 25, 2076-2080, 1989.

TECPLOT, TECPLOT - Version 6 - User's manual, Amtec Engineering, Bellevue, WA, 1995.

Roth, K., W.A. Jury, H. Flühler, W. Attinger, Transport of chloride through an unsaturated field soil, *Water Resour. Res.*, 27, 2533-2541, 1991.

Roth, K., Steady-state flow in an unsaturated, two-dimensional macroscopically homogeneous, Miller-similar medium, *Water Resour. Res.*, 31, 2127-2140, 1995.

Van Genuchten, M.T., A closed-form equation for predicting the hydraulic conductivity of unsaturated soil, *Soil Sci. Soc. Am. J.*, 892-898, 1980.

Wang, J.S.Y., Variations of hydrological parameters of tuff and soil, Proceedings of the Third Annual International High-Level Radioactive Waste Management Conference at Las Vegas, NV, 727-731, 1992.

Williams, S.A., A.I. El-Kadi, COVAR - A computer program for generating two-dimensional fields of autocorrelated parameters by matrix decomposition, Int. Groundwater Model. Cent., Holcomb Res. Inst., Butler Univ., Indianapolis, Ind., 1986.

Ernest Orlando Lawrence Berkeley National Laboratory
One Cyclotron Road | Berkeley, California 94720

Prepared for the U.S. Department of Energy under Contract No. DE-AC03-76SF00098